Tetrahedron Letters 60 (2019) 151021

Contents lists available at ScienceDirect

Tetrahedron Letters

journal homepage: www.elsevier.com/locate/tetlet

Digest paper

Molecular design of star-shaped benzotrithiophene materials for organic electronics

Saverio Santi *, Serena Rossi

Dipartimento di Scienze Chimiche, Università degli Studi di Padova, via Marzolo 1, 35131 Padova, Italy

ARTICLE INFO

Article history:
Received 27 May 2019
Revised 18 July 2019
Accepted 6 August 2019
Available online 9 August 2019

Keywords:
Benzotrithiophene
Molecular electronics
Organic photovoltaic devices
Organic field-effect transistors

ABSTRACT

Progresses in the design and application of conjugated small molecules, oligomers and polymers have empowered rapid development of organic electronic technology as an alternative to conventional devices. Among the numerous organic electronic materials, benzotrithiophene (BTT)-based oligomers and polymers have recently come in the limelight demonstrating great potential in organic electronics as high performance photovoltaic devices, field-effect transistors, electrochromic materials, high-area capacitors and charge carrier discotic liquid crystals. In this digest, we propose an overview of the organic electronic materials based on BTT isomers, highlighting the structure-performance relationship. The results obtained so far clearly indicate that the BTT isomers are among the most promising building blocks for the development π-extended materials for optoelectronic applications in the near future.

© 2019 Elsevier Ltd. All rights reserved.

Contents

Introduction . . . 1
Synthesis of BTT monomers . . . 2
Synthesis of **bbb-BTT-1** . . . 2
Synthesis of **bbb-BTT-2** . . . 3
Synthesis of **ccc-BTT** . . . 4
Synthesis of **bbc-BTT-3** . . . 4
Theoretical study on BTT isomers . . . 5
bbb-BTT-1 devices . . . 5
OPV devices . . . 5
OFET devices . . . 7
Electrochromic devices . . . 8
High-areal capacitors . . . 9
Charge carrier discotic liquid crystals . . . 10
bbb-BTT-2 devices . . . 10
OPV devices . . . 10
OFET devices . . . 12
bbc-BTT-3 devices . . . 13
BTT-based materials in perovskite solar cells . . . 14
Conclusion and outlook . . . 15
Acknowledgement . . . 17
References . . . 17

Introduction

Organic materials have emerged as powerful supplies for their numerous applications in molecular electronics, which include

* Corresponding author.
E-mail address: saverio.santi@unipd.it (S. Santi).

https://doi.org/10.1016/j.tetlet.2019.151021
0040-4039/© 2019 Elsevier Ltd. All rights reserved.

photovoltaic cells, field-effect transistors light-emitting diodes and supercapacitors [1].

Considerable attention has been devoted to thiophene-based π-conjugated organic materials due to their appropriate electronic, optical, and magnetic properties that make them efficient organic semiconductors [2]. The electron-donating character of thiophene and fused thiophene derivatives allowed for assembling donor-acceptor conjugated oligomers and polymers, and modeling their characteristics for applications in organic photovoltaic (OPV) cells [3], organic light-emitting diodes (OLEDs) [4], organic field-effect transistors (OFETs) [5] and electrochromics [6].

In particular, among the numerous OPV devices, benzodithiophene (**BDT**)-based materials have come to the fore in achieving exceptional power conversion efficiency (PCE) with the great potential in commercial applications [7].

Since 2003, great interest is emerged towards benzotrithiophene (**BTT**) isomers as potential π-cores for organic semiconductors. The rigid and planar conjugated structure of **BTT**s makes them attractive for achieving highly tunable molecular energy levels and optical band gaps as well as high hole-mobility. Moreover, the extended aromatic core due to the third fused thiophene is advantageous for intermolecular π-stacking and charge transport. Besides variations in the structure of the molecular backbone, organic material design has considered molecular shape and geometry [8], side chain effects [9], end-group contributions [10], and molecular-weight characteristics [11].

In particular, the three-dimensional functionalization of **BTT**s with side groups represents a viable and proficient method to improve the electronic performance of the resulting conjugated materials. Accordingly, the correlation between the molecular structure of the conjugated molecule and the device efficiency can be determined.

This digest is addressed to review the synthetic strategies, the chemical structures and the electronic properties of **BTT**-containing conjugated small molecules, oligomers and polymers developed over the past sixteen years:

i. the general synthetic routes of **BTT** units and conjugated materials are described;
ii. the design strategies of backbone modification, functional substitutions and side chain introduction are discussed;
iii. a wide range of **BTT**-based derivatives are introduced by application.

Finally, a brief review about challenges and perspectives of **BTT**-based material is presented.

Synthesis of BTT monomers

Among the seven possible **BTT** isomers, according to the positions of the sulfur atoms shown in Fig. 1, there is no report on benzo[1,2-*b*:-3,4-*c*':5,6-*c*"]trithiophene (**bcc-BTT**), benzo[1,2-*b*:-4,3-*b*':5,6-*c*"]trithiophene (**bbc-BTT-1**) and benzo[1,2-*b*:4,3-*b*':5,6-*c*"]trithiophene (**bbc-BTT-2**), probably owing to synthetic difficulties.

In reverse, the early syntheses of benzo[1,2-*b*:3,4-*b*':5,6-*b*"]trithiophene (**bbb-BTT-1**) [12], benzo[2,1-*b*:3,4-*b*':5,6-*b*"]trithiophene (**bbb-BTT-2**) [12b] benzo[1,2-*c*:3,4-*c*':5,6-*c*"]trithiophene (**ccc-BTT**) [13] have been achieved by oxidative photocyclization of terthiophenes (Scheme 1) or intermolecular cyclic condensation (Scheme 10).

More recently, the synthesis of the fourth member of the **BTT** family, the benzo[2,1-*b*:3,4-*b*':5,6-*c*"]trithiophene (**bbc-BTT-3**) was reported [14].

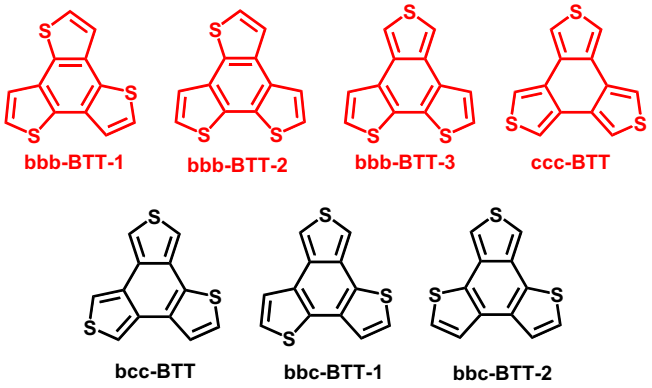
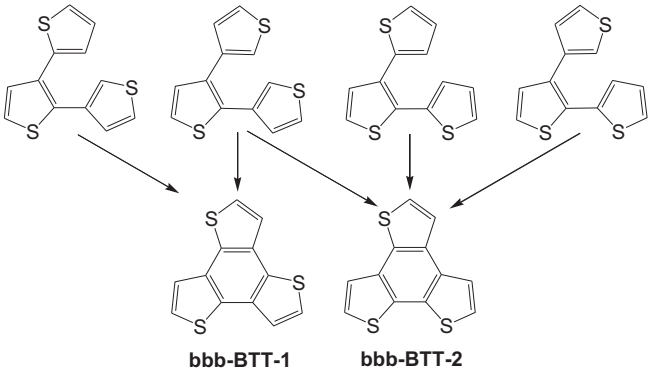


Fig. 1. The seven possible **BTT** isomers.



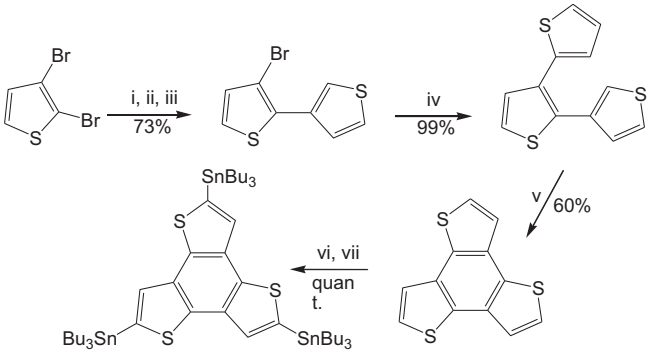
Scheme 1. Early synthesis of **bbb-BTT-1** and **bbb-BTT-2.**

The growing interest towards **BTT**-based organic electronics has encouraged the research of new members of the **BTT** family and more convenient synthetic methods of known **BTT** monomers.

*Synthesis of **bbb-BTT-1***

The **bbb-BTT-1** isomer has been thoroughly studied and mainly used as a core for the preparation of star-shaped oligomers, polymers, and dendrimers.

In 2004, Roncali synthesised **bbb-BTT-1** according to Scheme 2, starting from the commercially available 2,3-dibromothiophene (**3**). Modifications of the literature procedures allowed shortening



Scheme 2. Synthesis of **bbb-BTT-1** (i) *n*-BuLi (1 equiv) THF, -70 °C; (ii) tetrahydrothiophene, THF, -70 °C to reflux, the HCl (aq); (iii) chloranyl, ethileneglycol, reflux; (iv) 2-thienyl agnesiumbromide, $NidppeCl_2$, Et_2O, reflux; (v) *hv*, cat, I_2, O_2, toluene; (vi) *n*-BuLi (6 equiv), THF, 0 °C and the 20 °C; (vii) Bu_3SnCl.

time reaction and improvement of the overall yield (Scheme 2) [15].

The use of **bbb-BTT-1** as a rigid and planar central core bound to thiophene rings offers the possibility of building star-shaped oligothiophenes.

In 2011, Takimiya described the one-pot synthesis of substituted benzothiophenes from thioannulation of *o*-bromoethynylbenzenes in *N*-methyl-2-pyrrolidone (NMP) at 180 °C using sodium sulphide (Scheme 3a) [12c].

Similarly, reaction of 1,3,5-trichloro-2,4,6-tris[(*trimethyl-silyl*)*ethynyl*]-benzene gave **bbb-BTT-1** in good yield (60%, Scheme 4). Three-fold cyclization on the benzene ring to afford **BTT**s was not obtained before.

As reported by Sanz [16] and Zhang [17], the utility and applicability of the above reactions suffer from the harsh reaction conditions [18a].

Using the recently developed transition-metal-catalyzed reaction forming carbon-sulfur bond [19], in 2011 Zhang proposed a copper-catalyzed thioannulation reaction of bromoalkynylbenzenes with sodium sulphide, giving differently substituted benzo[*b*]thiophenes in the presence of CuI/TMEDA in DMF at 80 °C for 24 h in moderate and good yield (Scheme 3b) [17].

Our unsuccessful efforts to prepare of **bbb-BTT-1** following Takimiya and Zhang methods forced us to endeavor a modified synthetic strategy. In 2016, Li reported the transition-metal-free thiolation-annulation of 2-fluorophenylacethylene with sodium sulphide giving 2-phenylbenzo[*b*]thiophene (Scheme 5) in an outstanding 91% yield.

We applied this method to 1,3,5-trifluoro-2,4,6-tris[(*trimethylsilyl*)*ethynyl*]benzene, prepared from 1,3,5-trifluoro-2,4,6-triiodobenzene in 98% yield [18a], obtaining **bbb-BTT-1** in a discrete yield (45%). Finally, we improved the threefold thioannulation reaction of the fluorinated derivative in the presence of CuI/TMEDA in DMF, obtaining **bbb-BTT-1** in good yield (78%) and with a short reaction time (Scheme 6).

Similarly, we prepared the tris(ferrocenyl) derivative of **BTT**, the 2,5,8-tris(ferrocenyl)benzo[1,2-*b*:3,4-*b'*:5,6-*b''*]-trithiophene (**2**), the first examples of organometallic complex of **BTT** reported so far (Scheme 6) [18a].

The redox and optical properties of the cationic derivatives **Fc_3-BTT-1** and the related **Fc_2-BDT** were rationalized by an in-depth electrochemical and optical study [18b]. In particular, the near infrared spectra of the cationic species displayed typical charge transfer bands, which were rationalized in the framework of the Marcus-Hush theory. These species are well placed into the regime of rather strongly coupled mixed-valence systems, with metal-metal electronic coupling greater in **(Fc_3-BTT-1)$^+$** than in **(Fc_2-BDT)$^+$**.

In addition, the greater electronic coupling found for the thiolated compounds with respect to the sulfur-free trindene [18c] and indacene [18d] ferrocenyl derivatives demonstrated the huge influence of thiolation on the conjugative properties. The heteroatom effect is in agreement with the strong conductive properties of **BDT** and **BTT**, which are the basis of their preeminent application as organic materials.

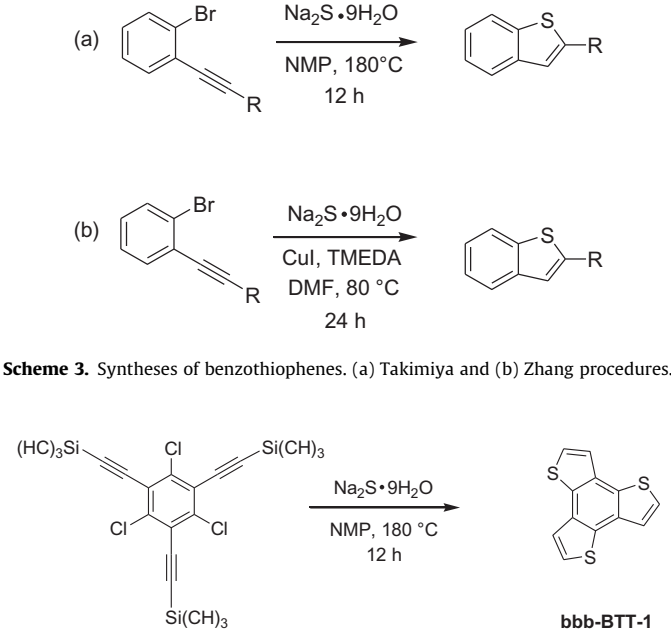
Alternative routes for the synthesis of **bbb-BTT-1** from 1,3,5-trichlorobenzene [6a], (several steps, long reaction times, 55% yield) or 1,3,5-trihydroxybenzene [20] (one-pot, 10% yield) have been reported.

*Synthesis of **bbb-BTT-2***

In contrast to **bbb-BTT-1**, in which the sulfur atoms are arranged *meta* with respect to the benzene unit, **bbb-BTT-2** allows for a direct conjugation between the two α-positions. Several functionalized **bbb-BTT-2** were synthesised by Nelsen [21] in 2011 in good overall yields and in three steps: starting from 2,3-dibromothiophene, a side chain was incorporated by a Friedel-Crafts acylation and the acyl-functionalized **bbb-BTT-2** was assembled by a Suzuki-Miyaura cross-coupling reaction with thiophene-3-boronic acid followed by ring-closing oxidation with DDQ (Scheme 7).

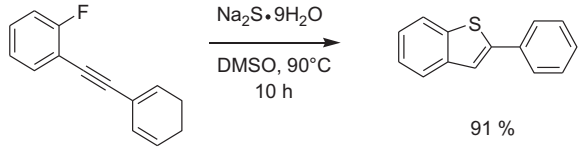
The acyl-functionalized BTT was easily converted to the corresponding alkyl-**BTT** (Scheme 8).

In order to functionalize the aryl derivative for subsequent introduction of the **bbb-BTT-2** system into π-conjugated polymers, the 2,8-dibrominated compounds were synthesised by forming the

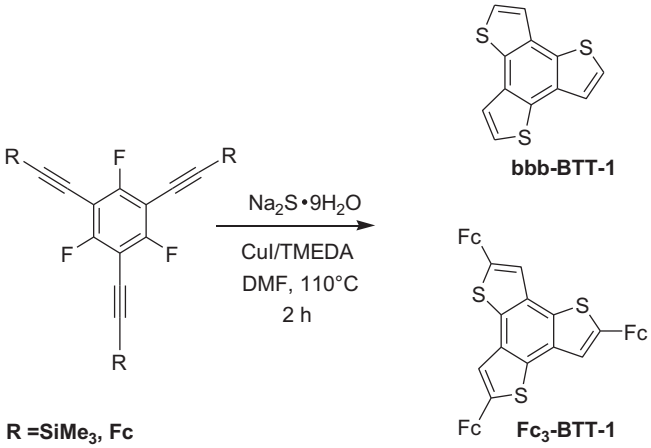


Scheme 3. Syntheses of benzothiophenes. (a) Takimiya and (b) Zhang procedures.

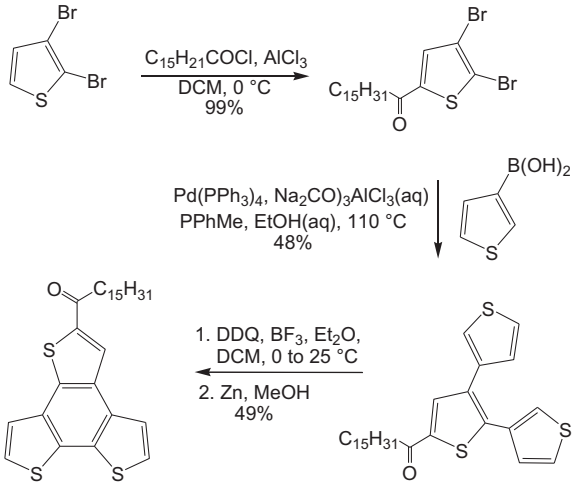
Scheme 4. Takimiya synthesis of **bbb-BTT-1**.



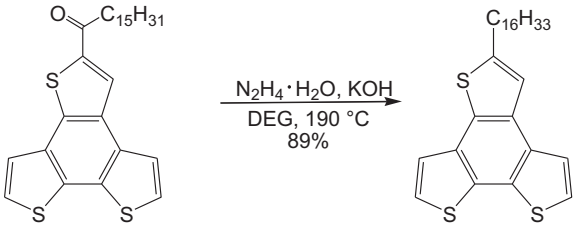
Scheme 5. Syntheses of -phenylbenzo[*b*]thiophene.



Scheme 6. Our alternative synthesis of **bbb-BTT-1**.



Scheme 7. Synthesis of acyl-functionalized **bbb-BTT-2**.

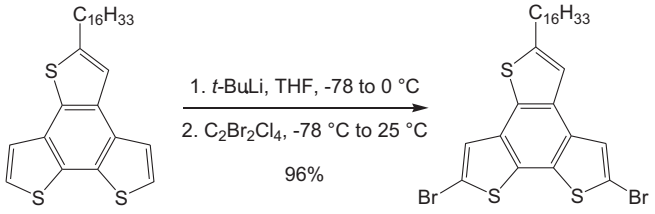


Scheme 8. Synthesis of alkyl-functionalized **bbb-BTT-2**.

2,8-dilithiated **bbb-BTT-2** with *tert*-butyllithium and subsequently reacting the dilithiated species with 1,2-dibromotetrachloroethane in very excellent yield (Scheme 9).

The solubilizing side chain contributes extra electron density to the aromatic backbone. The crystallographic structure, obtained with a shorter acyl chain ($C_8H_{17}CO$–) showed a fully planar geometry of the aromatic core. Moreover, the bonding geometry of the side chain, through the two unsubstituted α-positions of aromatic moiety, is associated with a ca. 140° bend (Fig. 2).

In a series of polymers, each containing one of the five different benzodithiophene isomers copolymerized with bithiophene, Müllen demonstrated the critical role of the different bonding



Scheme 9. Synthesis of 2,8-dibrominated alkyl-**bbb-BTT-2**.

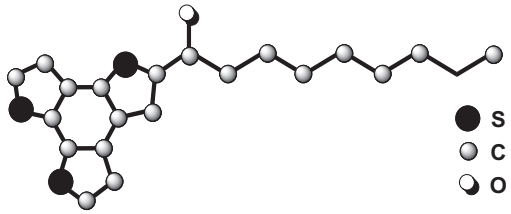


Fig. 2. Sketch of the $C_8H_{17}CO$-**bbb-BTT-2**, structure.

geometry of the benzodithiophene monomers in varying the degree of curvature introduced into the polymer backbone chain.

The curvature strongly influences solubility, electronic levels, morphology, and charge carrier mobility in OFET transistors. A high degree of curvature improves the solubility, but worsens the order in the film. As a guideline for design of semiconducting polymers, the polymer with an intermediate degree of curvature yields the highest charge-carrier mobility and adequate solubility [22].

The curvature found for the acyl **bbb-BTT-2** is similar to the best performing material in the Müllen study. Its fully planar and highly electron-rich aromatic system, with ideal backbone curvature for good charge mobility, makes it a promising candidate as a donor component in D-A copolymers for OPVs.

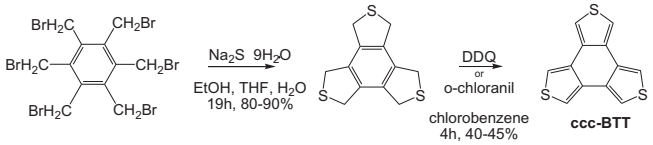
*Synthesis of **ccc-BTT***

In 1978, Hart synthesised **ccc-BTT** by refluxing a solution of hexakis(bromomethyl)benzene and sodium sulphide in a mixture of ethanol, THF and water, followed by dehydrogenation of the obtained dodecahydro-**ccc-BTT** with either DDQ or *o*-chloranil in chlorobenzene at reflux (Scheme 10) [13a].

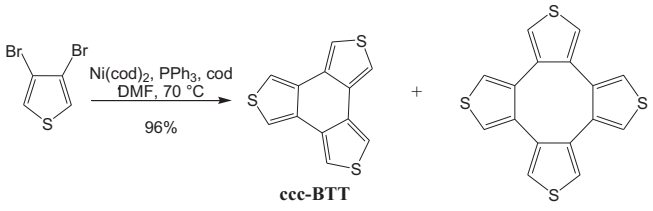
More recently, in 2007, Bendikov [13b] prepared **ccc-BTT** in 40% yield by one-pot coupling of 3,4-dibromothiophene with [Ni(cod)$_2$] in the presence of free 1,5-cyclooctadiene and PPh_3 in DMF (Scheme 11). The 3,4-dibromothiophene produced **ccc-BTT** and cycloocta[1,2-*c*:3,4-*c*′:5,6-*c*″:7,8-*c*‴]tetra-thiophene in a 1:1 ratio. **ccc-BTT** displayed unusual electronic structure and solid-state packing involving π–π stacking. Thus, important applications as OFET transistors are expected.

*Synthesis of **bbc-BTT-3***

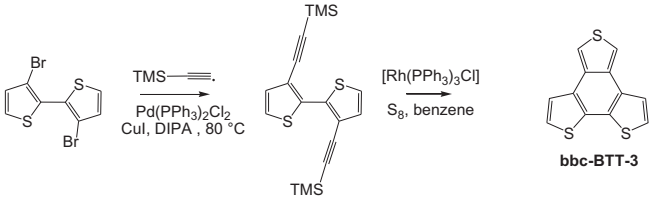
In 2011, Müllen [14] reported the synthesis of the last member of the **BTT** family, the benzo[2,1-*b*:3,4-*b*':5,6-*c*"]trithiophene (**bbc-BTT-3**) (Scheme 12). Starting from 3,3′-dibromo-2,2′-bithiophene, the TMS, substituted alkyne were introduced by Sonogashira reac-



Scheme 10. Early synthesis of **ccc-BTT**.



Scheme 11. Recent synthesis of **ccc-BTT**.



Scheme 12. Synthesis of **bbc-BTT-3**.

tions in 78% yield. Then, it was treated with Wilkinson catalyst ($Rh(PPh_3)_3Cl$) to produce a rhodium complex intermediate that were converted to **bbc-BTT-3** by adding sulfur powder (20%).

As shown by plenty of organic electronic materials developed and applied over the past few decades, the subtle variations in the molecular structures of conjugated molecules leads to significant changes in the electronic properties.

Thus, comprehension of the relationship between molecular structure and electronic performance remains a challenge.

Theoretical study on BTT isomers

In the following sections, we will summarize the molecular design strategies of **BTT**-containing materials, namely **bbb-BTT-1**, **bbb-BTT-2** and **bbc-BTT-3,** for applications in organic electronics. According to DFT calculations, the HOMO energy levels increase in the order **bbb-BTT-1** < **bbb-BTT-2** < **bbc-BTT-3**, providing a theoretical support for increasing electron-rich donor capability [14].

Liu and Zhang [23], employing many-body perturbation theory (MBPT), explored the effects of the sulfur atoms configuration on the molecular structures and the electronic properties of five conjugated copolymers, containing **BTT** isomers as donor units and benzothiadiazole (BTZ) as acceptor units, connected by thiophene spacers (**bbc-BTT-3-BTZ**, **bbb-BTT-2-BTZ**, **bbc-BTT-1-BTZ**, **bbc-BTT-2-BTZ** and **bcc-BTT-BTZ**).

In particular, **bbc-BTT-3-BTZ**, **bbb-BTT-2-BTZ**, the unique polymers containing existing **BTT** isomers, displayed the best coplanarity with the lowest dihedral angles between the two neighboring rings.

In addition, they revealed intense adsorption at the highest wavelengths 660 and 623 nm, respectively, indicating their promising application in solar cells. The increasing of the effective conjugation lengths was suggested to originate the red shift of about 150 nm from **bcc-BTT-BTZ** to **bbc-BTT-3-BTZ**.

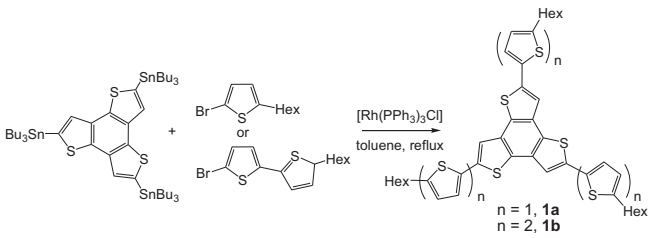
Compared with the linear thiophene-based donors, such as the above-mentioned benzodithiophene, the fully planar and extended aromatic system of **bbc-BTT-3** should facilitate the formation of highly ordered and self-organized structures, which are particularly important for OFET application [24].

bbb-BTT-1 devices

Roncali's group reported syntheses [15] and noteworthy performances in photovoltaic devices [3d] of star-shaped oligothiophenes based on the **bbb-BTT-1** core. Compared to the benzene-core derived oligomers, the enhanced semiconducting properties were attributed to the increased planarity of these derivatives. From then on, many efforts were devoted to the preparation of small molecule, oligomers and polymers based on **bbb-BTT-1**, and their applications as OPV, OFET, high-areal capacitive, electrochromic and charge-carrier devices.

OPV devices

Planarized star-shaped oligothiophenes based on **bbb-BTT-1** were prepared by Roncali [15], according to Scheme 13. In a star-shaped oligothiophene, obtained by direct functionalization of a central benzenic core with at least three oligothiophene chains [25], the steric interactions produce a dihedral angle between benzene and thiophene rings, limiting the effective conjugation [25a-d, g]. Otherwise, the dihedral angle between two consecutive thiophene rings is close to 0° [26].



Scheme 13. Synthesis of oligothiophenes based on **bbb-BTT-1**.

Therefore, the **BTT** core allowed the preparation of planar star-shaped oligothiophenes with enhanced π-electron delocalization.

Compounds **1a** and **1b** (Scheme 13) were obtained by a threefold Stille reaction between the tris(stannyl) derivative and 2-bromo-5-*n*-hexylthiophene **9** or 5-bromo-5′-*n*-hexyl-2,2′-bithiophene **12**, respectively, in the presence of a catalytic amount of $Pd(PPh_3)_4$.

The electronic properties of the star-shaped compounds **1a**, **1b** and of the corresponding linear reference compounds **2a** and **2b** (Fig. 3) have been examined by cyclic voltammetry (CV) and UV–vis spectroscopy (Table 1) [3d].

Oxidative CV analysis indicated that (i) the star-shaped arrangement significantly stabilizes the radical cations, (ii) the presence and lengthening of the oligothiophene chain(s) induce a negative shift of the anodic potential due to the conjugation extension, (iii) the significant negative shift of potentials in star-shaped **1** molecules is indicative of an increase of the HOMO levels.

In addition, UV–vis spectra showed a bathochromic shift of λ_{max} in star-shaped **1** with respect to linear **2** systems indicating a decrease of the HOMO-LUMO energy gap (Table 1).

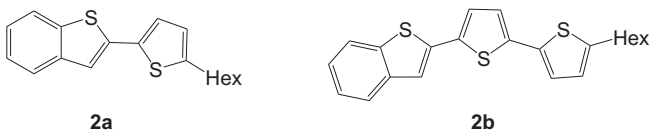
Finally, the thermal stability of star-shaped systems resulted much higher than that of the linear analogues, and they could be processed by vacuum sublimation without degradation.

The solution spectra of **1b** and **2b** displayed a red shift of the λ_{max}, from 379 nm for the linear compound **2b** to 405 nm for the star-shaped compound **1b**. This low-energy shift was attributed to the combined effects of higher planarity and stiffness of the **bbb-BTT-1** core, leading to an enhancement of the π-electron delocalization related to a decrease of HOMO-LUMO gap.

Comparison with the solid-state spectra of compounds **1b** and **2b** as thin solid film sublimed on glass reveals very different behaviors.

For compound **2b**, solid deposition yields a blue shift of λ_{max} from 379 to 319 nm and the appearance of a weak new transition at 417 nm.

The spectral features correlate with a vertical orientation of the molecules on the surface. In particular, the splitting of the excited singlet was attributed to the exciton interactions between adjacent molecules in a close- packed organization. Differently, the solid-state spectra of **1b** displayed a red shift of λ_{max} from 405 to 420 nm and the appearance of a vibronic fine structure.



2a **2b**

Fig. 3. Reference thiophene derivatives.

Table 1
Electrochemical, optical and thermal data for **1** and **2**.

Compound	E_{pa}/V[a]	λ_{max}/nm[b]	$T_d/°C$[c]
1a	1.16	357	405
1b	0.93	404	430
2a	1.30	326	185
2b	1.15	379	232

[a] Compound 0.1 mM in 0.2 M Bu_4NPF_6/CH_2Cl_2, Pt electrodes vs Ag/AgCl, scan rate = 100 mV/s.
[b] In CH_2Cl_2.
[c] Temperature of decomposition.

These features were interpreted by supposing a parallel orientation to the surface. These conclusions were confirmed by the X-ray diffraction (XRD). Additionally, the absorbance of the film of **1b** was three times larger than that of **2b**.

These properties, associated with the enhanced π-electron delocalization characteristic of the fused star-shaped core, led to a considerable performance improvement of **bbb-BTT-1-** containing OPV cells.

In fact, bulk heterojunction (BHJ) solar cells were realized on ITO substrates spin-coated with a film of Baytron P, (a water-dispersable polymer complex between poly(3,4-ethylene dioxythiophene), **PEDOT**, and polystyrene sulfonic acid with donor (**1b** or **2b**) and acceptor (N,N'-bis-tridecyl-perylene-dicarboxyimide) layers sublimed under vacuum. With **1b**, the cell showed much higher PCE than that with **2b** (1.14 vs 0.1%).

These results clearly indicate that the considerable differences between the redox and optical properties of **1b** and **2b,** as well as the structure of their sublimed thin films, have a crucial role for the efficiency of the remarkable performance in corresponding photovoltaic devices.

The effect on OPV performance of BHJ solar cells, by increasing the number of thiophene units connecting to star-shaped **bbb-BTT-1**, was further verified.

Xiao [27] investigated the photovoltaic application of three structurally closely related small molecules, **BTT-BTD-0**, **BTT-BTD-1** and **BTT-BTD-2**, with 0, 1, 2 thiophenes connecting BTT core to the electron deficient benzo[2,1,3]thiadiazole (**BTD**) arms (Fig. 4), using fullerene derivatives as electron acceptor.

The molecules bearing more thiophene units between the **BTT** core and the **BTD** arms possessed higher-lying HOMO levels while their LUMO levels remain practically unaffected, accordingly to their optical and electrochemical properties (optical band gap potentials and onset oxidation in solution and thin film), and DFT calculations.

The more thiophenes there were, the better the performance of related solar cells up to a PCE value of 1.36%.

A successful example of improving fullerene-free polymeric solar cells performance was reported by Chen [28a].

New **bbb-BTT-1**-based electron acceptor were synthesised, **TriPDI** and **Fused-TriPDI** (Scheme 14), in which three perylene diimide (PDI) moieties are bound to a **bbb-BTT-1** core via single bonds (**TriPDI**) or ring-fusion (**Fused-TriPDI**).

The **TriPDI** showed a highly twisted skeleton through the single bonds whilst **Fused-TriPDI**, exhibited good structural rigidity, planarity and actual conjugation between PDI and **bbb-BTT-1**. As a result, **Fused-TriPDI** displayed higher optical band gaps and HOMO-LUMO energy levels, stronger UV–vis absorption and charge mobility one order of magnitude greater than **TriPDI**.

Poly[4,8-bis(5-(2-ethylhexyl)thiophen-2-yl)benzo[1,2-*b*;4,5-*b*'] dithiophene-2,6-diyl-*alt*-(4-(2-ethylhexyl)-3-fluoro-thieno[3,4-*b*] thiophene)-2-carboxylate-2,6-diyl] (PTB7-Th) was employed as the donor to construct polymeric solar cells. The devices based on **Fused-TriPDI** exhibited PCE of 6.19%, almost three times higher than the value of 2.19% found with **TriPDI** (1.15% according to other authors [28b]). The better performance was mainly attributed to the increased electron mobility in the rigid and planar skeleton of **Fused-TriPDI**.

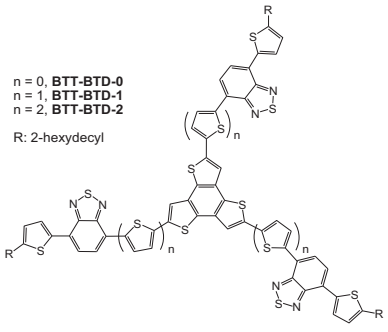
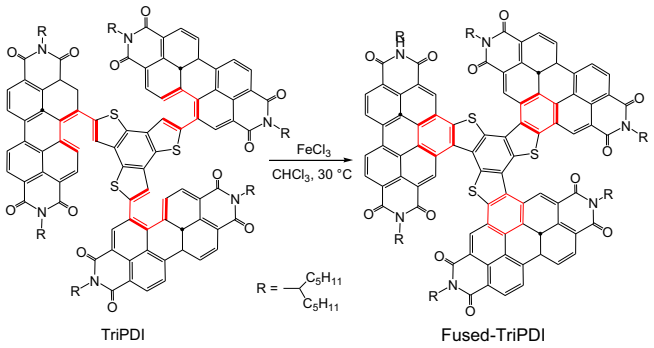


Fig. 4. **BTD**-containing oligothiophenes based on **bbb-BTT-1.**



Scheme 14. Synthesis of PDI-based **bbb-BTT-1** derivatives.

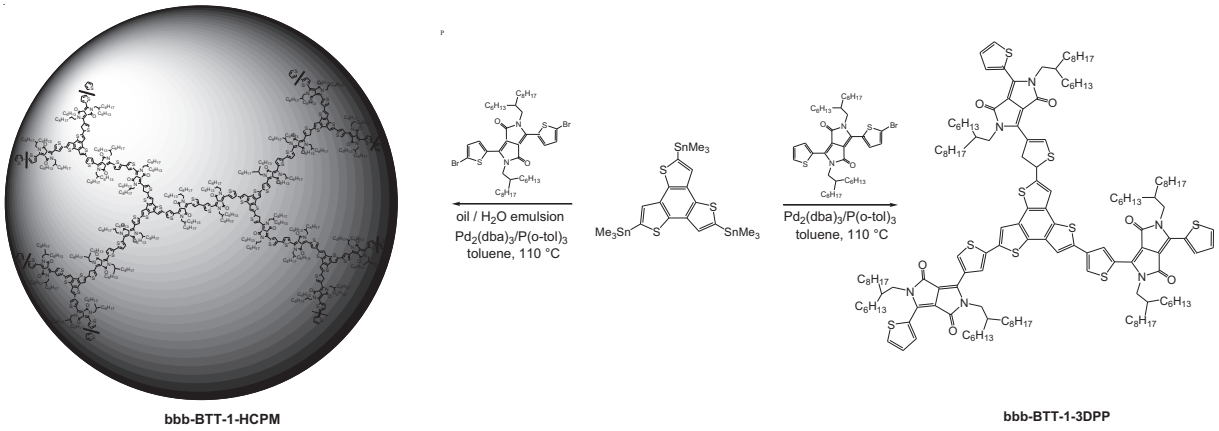
The high structural C_{3h}-symmetry and planarity of **bbb-BTT-1** allow 2D molecular conjugation, facile π-stacking and formation of 3D structures, such as star-shaped molecules, dendrimers, and hyperbranched polymers. However, **bbb-BTT-1** has mostly been used for construction of star-shaped π-conjugated molecules [3d,6a,15,27,29–31] and dendrimers [12d], and the development of hyperbranched polymers based on **bbb-BTT-1** has been severely limited due to difficult processibility. Recently, the star-shaped **bbb-BTT-1-3DPP**, based on **bbb-BTT-1** with three diketopyrrolopyrrole (DPP) arms, has displayed good planarity and extended π-conjugation, although its PCE was rather low (0.29%) [29].

In 2017, Wang and Tong [32] reported the preparation of solution-processible nanoparticles (**bbb-BTT-1-HCPN**s) (Scheme 17), with tunable particle sizes, of a hyperbranched conjugated polymer based on **bbb-BTT-1** and DPP, via Stille miniemulsion polymerization with hexadecyl trimethyl-ammonium bromide (CTAB) as surfactant (Scheme 15).

The average particle sizes increased from 50 (**BTT-HCPN-1**) to 80 nm (**BTT-HCPN-2**) when the reaction time changed from 1 to 4 h. The UV–vis spectra of **BTT-HCPN-1** and **BTT-HCPN-2** showed strongly red shifted and broader absorption bands in both solution and thin film than **BTT-3DPP**. In particular, **BTT-HCPN**s in solution and thin film showed extended absorption up to 1000 nm, indicating strong intramolecular aggregation of π-conjugated chains in **BTT-HCPN** particles even in dilute solutions. The larger **BTT-HCPN-2** showed the broader and more red-shifted absorption band than **BTT-HCPN-1**, suggesting stronger aggregation inside the larger particle.

The optical band gaps estimated from the absorption onset wavelengths for **BTT-HCPN-1** and **BTT-HCPN-2**, (1.42 and 1.38 eV, respectively) were much smaller than that of **BTT-3DPP** (1.83 eV), suggesting more efficient light harvesting of **BTT-HCPN**s. In fact, the broadest and reddest shifted absorption of **BTT-HCPN-2** were in agreement with the performances of optimized solar cells based on **BTT-HCPNs**/PC71BM and **BTT-3DPP**/PC71BM. The highest short-circuit current and the best device performance were obtained for **BTT-HCPN-1** and **BTT-HCPN-2** with PCE of 1.51% and 1.46%, respectively, after treatment with 1,8-diiodooctane as a solvent additive, much higher than that of **BTT-3DPP** (0.31%).

If processing methods for p-type organic materials were commonly reported, efficient solution processed *n*-type materials of high dimensions are rare [33]. In particular, to our knowledge



Scheme 15. Synthesis of hyperbranched conjugated polymer nanoparticle **bbb-BTT-1-HCPN** and star-shaped small molecule **bbb-BTT-1-3DPP**.

two examples have previously been presented [34], only one containing the **bbb-BTT-1** core [35].

In 2018, Chochos reported a new solution processable *n*-type all conjugated polymer network (**PNT1**), in which three naphthalenediimide are connected to **bbb-BTT-1** (Fig. 5) [35].

The photovoltaic parameters of conventional (p-type) and inverted (*n*-type) devices indicated higher performance when **PNT1** was chosen as the electron acceptor in the inverted (*n*-type) device configuration with respect to the conventional (p-type) arrangement, in which **PNT1** was the electron donor (PCEs 0.3% and 1.2%, respectively). Although the absolute efficiencies were modest, operative photovoltaic devices were realized showing the potential use of this new type of material.

A novel small molecule **BTTCN** based on **bbb-BTT-1** (Fig. 6) was synthesised by Wang and Zu in 2018 [36].

Efficient OPV devices were assembled by incorporating a low amount of **BTTCN** into the blend film, together with a fullerene derivative PC71BM as acceptor and a PTB7-Th polymer as donor. In this configuration, a cascade energy level alignment was observed, in which the **BTTCN** plays a bridging role as an energy cascading dopant and provides additional pathways for exciton dissociation in the bulk heterojunction films. An optimized PCE value of 9.43% was obtained with a minimal amount of **BTTCN** (3%).

OFET devices

Takimiya synthesised **bbb-BTT-1** planar oligomers up to a dendritic decamer (**2**–**6**) [12d].

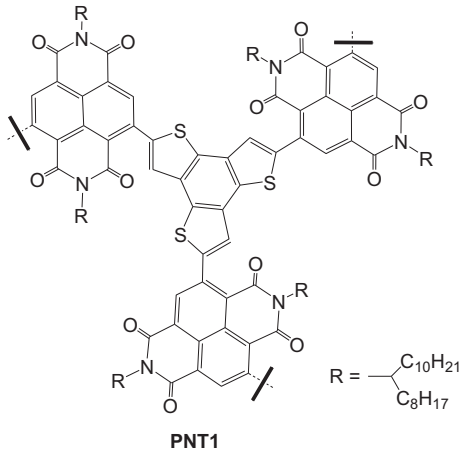


Fig. 5. Polymer network **PNT1.**

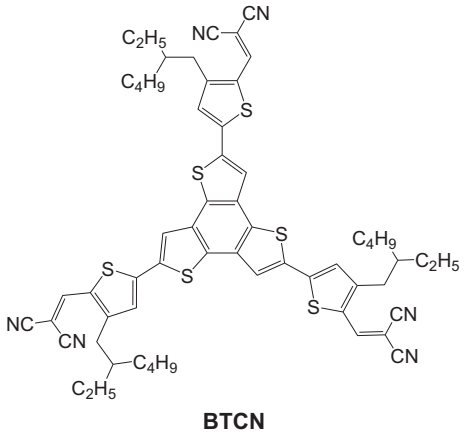


Fig. 6. Star-shaped conjugated small molecule **BTCN**.

A series of intermediates was prepared as building blocks for the modular synthesis of the final compounds (Fig. 7). The dimers **(BTT-1H)$_2$** and **(BTT-1R)$_2$** were prepared by monolithiation of **bbb-BTT-1** and dioctyl-**bbb-BTT-1** followed by oxidative coupling with Fe(acac)$_3$ (Scheme 16).

A tetramer **(BTT-1)$_4$**, was obtained employing the palladium-catalyzed Stille reaction between trimethylstannyl and tribromide **bbb-BTT-1** derivatives (Scheme 17).

For further oligomerization, the trimeric bromine and trimethylstannane dendron units were similarly prepared (Scheme 18).

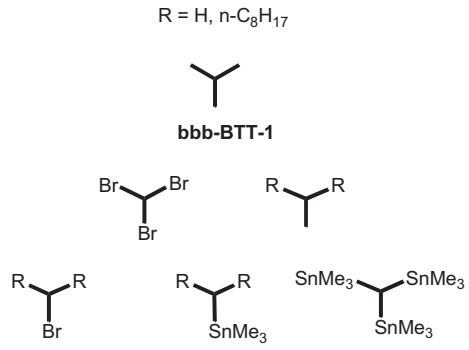
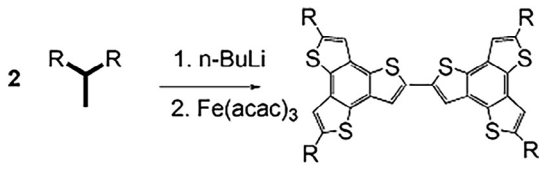
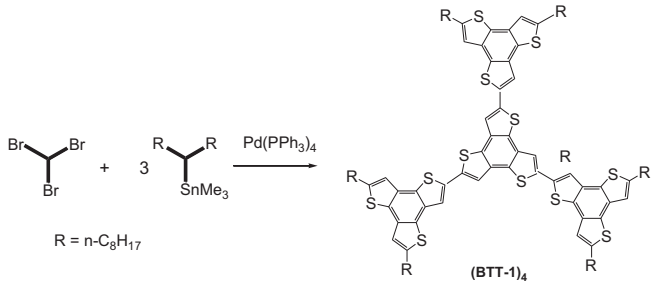


Fig. 7. Building blocks for modular synthesiss of **bbb-BTT-1** oligomers and dendrimers.

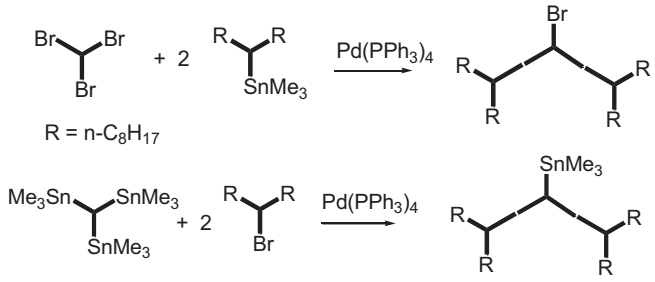


(BTT-1H)$_1$, R = H; **(BTT-1R)$_2$**, n-C_8H_{17}

Scheme 16. Synthesis of **bbb-BTT-1** dimers.

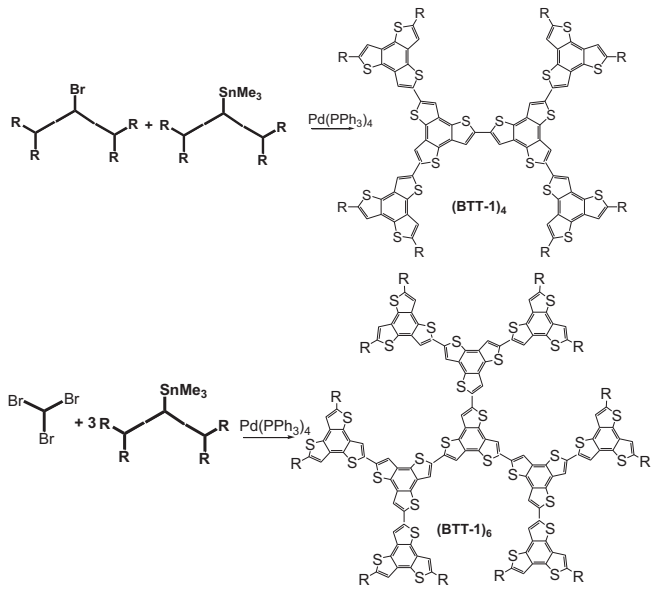


Scheme 17. Synthesis of **bbb-BTT-1** tetramers.



Scheme 18. Synthesis of **bbb-BTT-1** dendrons.

Their combination with the appropriate stoichiometric ratio gave the hexamer **(BTT-1)$_6$** and the decamer **(BTT-1)$_{10}$** (Scheme 19).



Scheme 19. Synthesis of **bbb-BTT-1** hexamer and decamer (R = C_9H_{17}).

Their π-stacking crystal structures, irrespective of the absence or the presence of peripheral octyl groups, indicated that **bbb-BTT-1** core guarantees an intermolecular structure for developing new π-conjugated functional materials. The stability and solubility of the alkylated oligomers made them suitable for deposition and characterizations of their thin films.

The estimation of the HOMO energy levels and HOMO-LUMO gaps through their CV oxidation potential, UV–vis absorption spectra and DFT calculations indicated that their electronic structures were not strongly affected by the number of the **bbb-BTT-1** units in the oligomer but by the extent of orbital delocalization over the **bbb-BTT-1** units.

In the UV–vis spectra, the thin films of **(BTT-1R)$_2$** and **(BTT-1)$_4$** displayed red shifts which is an indication of intermolecular π-overlap between the planar molecules in the thin film state, as observed in the crystal structure of **(BTT-1R)$_2$**. This shift decreases for larger oligomers **(BTT-1)$_6$** and **(BTT-1)$_{10}$** due to their nonplanar geometry, which may prevent intermolecular structure suitable for actual carrier transport. In addition, only **(BTT-1R)$_2$** showed clear XRD peaks, indicative of formation of a crystalline thin film.

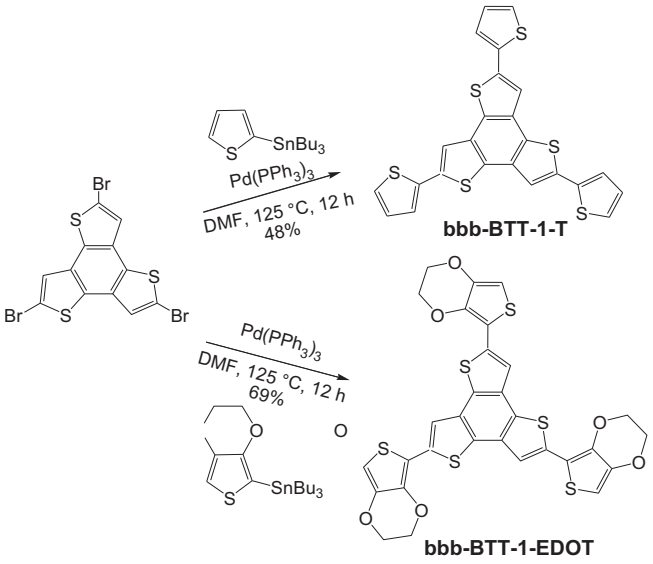
The molecular ordering in the thin film state of **(BTT-1R)$_2$** behaved as the active semiconducting layer in OFETs, with hole-mobility (0.14 $cm^2\ V^{-1}\ s^{-1}$) higher than that based on the larger oligomers **(BTT-1)$_6$** and **(BTT-1)$_{10}$** ($7 \times 10^{-4}\ V^{-1}\ s^{-1}$) owing to the amorphous nature in the thin film state of the latters. These results indicated that **bbb-BTT-1** core is a potential building block in developing new π-extended materials for optoelectronic applications and suitable as p-channel semiconductors. The control of morphology in the solid state is one of the key issues.

Electrochromic devices

Star-shaped **bbb-BTT-1-T** and **bbb-BTT-1-EDOT** derivatives of **bbb-BTT-1**, containing three thiophene and three EDOT (EDOT = 3,4-ethylenedioxythiophene) groups respectively, were obtained by Perepichka (Scheme 20) [6a].

The UV–vis absorption appearing at λ_{max} = 260 nm for **bbb-BTT-1**, typically attributed to HOMO-LUMO transition, was predictably red-shifted (343 nm) for thiophene-capped **bbb-BTT-1-T** and even more (355 nm) for EDOT-capped **bbb-BTT-1-EDOT**.

Polymer films of **bbb-BTT-1**, **bbb-BTT-1-T** and **bbb-BTT-1-EDOT** were generated on platinum electrode by multiple oxidative



Scheme 20. Synthesis of **bbb-BTT-1-T** and **bbb-BTT-1-EDOT**.

CV scans around the monomer potentials 1.39, 1.12 and 0.78 V vs Ag/AgCl, respectively. Poly(**bbb-BTT-1**) rapidly decomposed during multiple CV scans in propylene carbonate or benzonitrile. Poly (**bbb-BTT-1-T**) film was electrochemically stable in propylene carbonate, but slowly degraded in benzonitrile. Surprisingly, the poly (**bbb-BTT-1-EDOT**) exhibited stability upon oxidation in both solvents even in air-saturated electrolyte solution.

UV–vis experiments on poly**(bbb-BTT-1-T**) and poly(**bbb-BTT-1-EDOT**) on ITO transparent electrode and DFT calculation demonstrated that the HOMO and LUMO are localized between the benzene rings and slightly affected by the increasing polymerization number after dimerization. EPR spectra of the stable *p*-doped poly(**bbb-BTT-1-EDOT**) films, obtained by electrochemical oxidation at 1.0 V, showed an intense symmetric signal ascribed to a polaron. Increasing the doping level at a higher oxidative potential created more polarons in the polymers, leading to higher intensity of the EPR signal. On the contrary, polyEDOT **(PEDOT)** films showed a decrease of the EPR intensity at higher doping level due to the formation of low-spin bipolarons [37].

The single polaron nature of the charge carriers in poly(**bbb-BTT-1-EDOT**) was demonstrated by an UV–vis-NIR spectroelectrochemical experiment. A net electrochromic switching between the neutral (red) and doped (blue) polymer was observed. Gradually increasing of the potential from 0 to 1 V, the band at 480 nm disappeared and two new bands grew at 680 and 1316 nm. Actually, the characteristic isosbestic point at 548 nm indicating a distinct transition from the neutral to radical cation/polaron polymer, proved the formation of a polaron state.

Two octupolar organoboron compounds, 1,3,5-tris[5-(*dimesitylboryl*)*thiophen*-2-*yl*]terthienobenzene (**BTh-bbb-BTT-1**) and 1,3,5-tris[4-(*dimesitylboryl*)*phenyl*]terthienobenzene (**BPh-bbb-BTT-1**), bearing a **bbb-BTT-1** core as electron donor and dimesitylboryl groups as electron acceptors, were reported by Liu [30]. Both these derivatives exhibited strong blue-green fluorescence in common solvents under single or two photon excitation, with high quantum yields and good photo- and thermo-stability. However, the intensities of the two-photon excited fluorescence (TPEF) are lower than those of the single-photon excited fluorescence (SPEF) because the two-photon absorption is a low-probability third-order nonlinear optical absorption process. Since the effective charge-transfer region may be limited between boron-centered acceptor and the **bbb-BTT-1** core, the donor-acceptor bridge should be extended to obtain larger cross section of two-photon absorption. The TPEF values are not exceptional but analogous to those found for similar compounds.

High-areal capacitors

Electrochemical copolymerization of star-shaped **bbb-BTT-1** and **bbb-BTT-1-EDOT** with EDOT (Fig. 8) yielded high-surface-area π-conjugated networks with high areal capacitance [38].

The authors clarified the essential differences between electropolymerized homopolymer and copolymer networks made from these two building blocks. In fact, poly(**bbb-BTT-1-EDOT/EDOT**) frameworks attained an areal capacitance of 443.8 mF cm^{-2} (at 1 mA cm^{-2}), higher than those achieved by the respective homopolymers, poly(**bbb-BTT-1-EDOT**) and **PEDOT**, in the same experimental conditions of electrodeposition. Poly**(bbb-BTT-1-EDOT/EDOT**) displayed ca. 30-fold capacitance compared to **PEDOT**, attributed to the highly porous hierarchical π-conjugated frameworks formed during the electropolymerization. In addition, both poly(**bbb-BTT-1-EDOT**) and poly(**bbb-BTT-1-EDOT/EDOT**) frameworks were found to be resilient to repeated electrochemical cycling, with capacitance up to 89% over 1000 cycles), making them promising systems for high life cycle capacitive electrode applications.

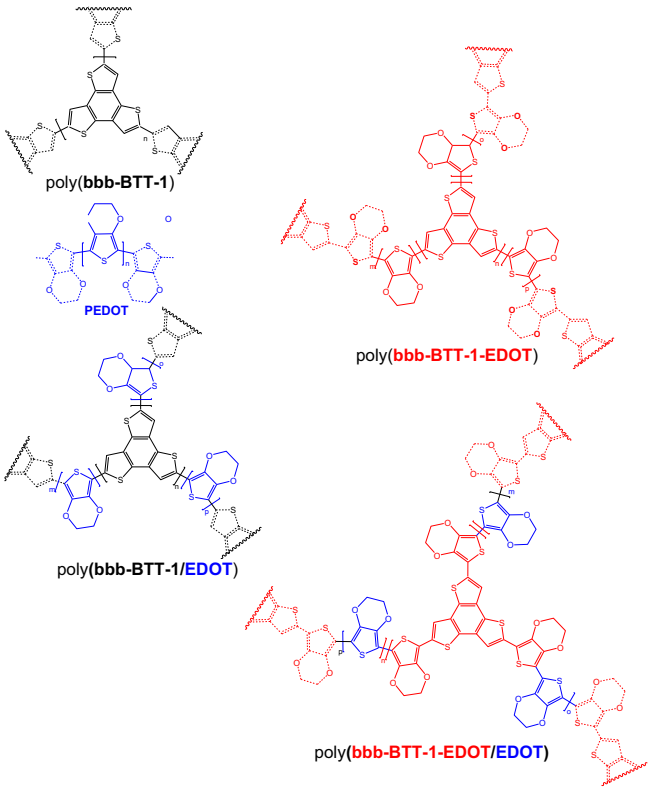


Fig. 8. Electropolymerized homopolymer and copolymer networks of **bbb-BTT-1** and **bbb-BTT-1-EDOT** with EDOT.

In 2018, Hao synthesised for the first time a C3-symmetric tricarbaldehyde of **bbb-BTT-1**, and built **bbb-BTT-1**-based covalent organic frameworks (COFs) of different pore sizes [39].

Notably, these COFs display great potential in visible-light photocatalysis and high-voltage supercapacity. By reaction of three aminobenzene derivatives, 1,3,5-Tris(4-aminophenyl)benzene (DADP), 1,4-diaminobenzene (DAB) and 1,3,5-Tris(4-aminophenyl)benzene (TAB) with **bbb-BTT-1**-tricarbaldehyde, BTT-COFs with different pore sizes (**BTT-DADP COF**, **BTT-DAB COF** and **BTT-TAB COF** were obtained (Fig. 9).

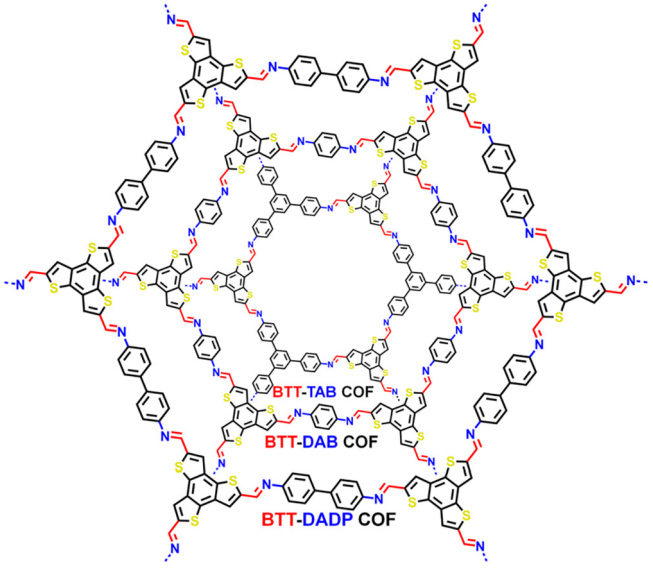


Fig. 9. bbb-BTT-1-based COFs with different pore sizes. Reprinted with permission from Wei, H.; Ning, J.; Cao, X.; Li, X.; Hao, L. *J. Am. Chem. Soc.* **2018**, *140*, 11618–11622. Copyright (2018) by the American Chemical Society.

Indeed, from **BTT-DADP COF**, to **BTT-DAB COF**, to **BTT-TAB COF**, the layered structures of COFs were revealed by the TEM measures, which suggested that the pore sizes of the COFs gradually become smaller and showed good potential for visible-light photocatalysis with optical band gaps of 2.04–2.08 eV.

The relatively poor conductivity of COFs hinders their broader applications. To enhance the conductivity of the COFs for electrochemical applications, the COFs were treated under ionothermal conditions with $ZnCl_2$ at 700 °C (the $ZnCl_2$ might have the function of padding and supporting the pore structures of the materials during the treatment). Nitrogen adsorption-desorption measurements revealed that the specific surface areas and the average pore sizes of COF-700 s became larger, in contrast with that of the COFs.

The electrochemical performances of COF-700 s were characterized by a symmetric supercapacitor system with an ionic liquid as the electrolyte. The cyclic voltammetry and the galvanostatic charge-discharge curves showed the typical double-layer supercapacitor characteristics of COF-700-based supercapacitors. This method appears exceptionally useful for the enhancement of electrochemical performances.

Charge carrier discotic liquid crystals

Self-organized columnar stacks of aromatic compounds, such as discotic liquid crystals [40,41], are an emergent class of organic semiconductors due to their intrinsic charge carrier mobility in bulk samples along the columnar stacking [41,42]. In addition, discotic liquid crystals are promising self-healing and highly anisotropic materials.

Charge carrier mobility generally decreases with decreasing order of the mesophases. Marcus theory provides a description of the dependence of the charge carrier mobility (electron hopping) on intermolecular electronic interactions [43] and predicts an increase in hopping rate with increasing electron transfer integral, which is a function of frontier-orbital overlap of adjacent molecules, and decreasing reorganization energy. An increase in temperature usually leads to an increase of the stacking distance, translational mobility and changes in rotational angle of stacked π-systems, causing a decrease in electron transfer integral.

Intermolecular formation of H-bonded in discotic molecules controls and well defines the columnar stacking distance and the relative orientations and locations. These systems are ideal materials for probing this model because are controlled by H-bonds and, consequently, well defined.

In this context, Perepichka and Eichhorn prepared the N,N',N"-(3,4,5-tridodecyloxyphenyl)tricarboxamide-**bbb-BTT-1** (Fig. 10) and reported its unique properties as a new H-bonded discotic liquid crystal [44].

The incorporation of three amide groups allowed for holding the molecules together in columnar stacks, favoring the formation of two thermotropic H-bonded hexagonal columnar mesophases (Col_h) in a temperature range from −50 to 280 °C, and suppressing the crystalline phase.

The charge carrier mobility was measured by time-resolved microwave conductivity in both Col_h mesophases.

The quasi-temperature independence found for the charge carrier mobility was explained by the interplay between stacking distance and mutual rotation due to the persistence of the intracolumnar H-bonds between amide groups.

bbb-BTT-2 devices

Since the successfully synthesis of the first polymer containing **bbb-BTT-2-**donor unit for application in OPV [45] and OFET [24b] devices, several studies were carried out in order to improve efficiency and performance of these materials.

OPV devices

The use of planar electron-donating molecules containing alternating units of electron donor and acceptor molecules can lower the material band gap and broad the absorption band towards longer wavelength. Simultaneously, the D-A architecture allows the manipulation of the energy levels of HOMO and LUMO [46]. In fact, the improvement of new light-harvesting donor materials for this type of solar cells requires careful adjustment of frontier-orbital energies [47]. This may guarantee more efficient donor-acceptor charge transfer and improve the intrinsic compromise between two desirable but incompatible features, a high open-circuit potential and an advantageous spectral overlap with the solar radiation [48].

The first **bbb-BTT-2**–containing copolymer (**P1**), bearing the **BTT** core as the donor and 2,1,3-benzothiadiazole (BTZ) as strong acceptor (Fig. 11), was successfully synthesised by Nielsen in 2011 [45]. **P1** behaved as a highly soluble and high molecular weight copolymer with a band gap of 1.75 eV, and performed in a cell for BHJ solar cells with fullerene-based electron acceptors, with a moderate PCE of 2.2% and a high open circuite voltage of 0.81 V when $PC_{71}BM$ was used.

DFT calculations predicted for **bbb-BTT-2** donor strength similar to the well-known benzodithiophene (**BDT**). In fact, for methyl-substituted BTZ and **bbb-BTT-2-BTZ** trimers, calculations envisaged moderate band gaps and low HOMO values, with **bbb-BTT-2** and bdt acting as weak donors.

In addition, **bbb-BTT-2** is helpful in promoting suitable intermolecular π-stacking interactions and the curvature of the polymer backbone induced by the bonding geometry of the side chain through the **BTT** moiety (Fig. 2) promoted polymer solubility and flexibility [22,24].

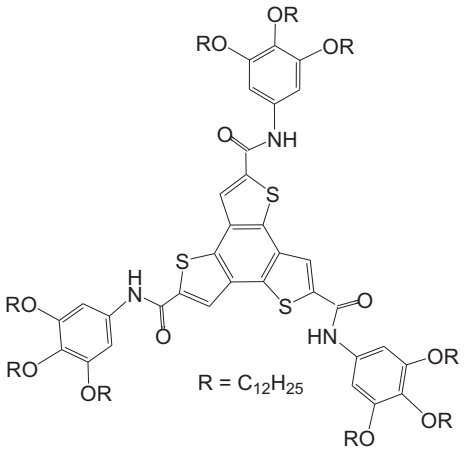


Fig. 10. N,N',N"-(3,4,5-tridodecyloxyphenyl)tricarboxamide-**bbb-BTT-1**.

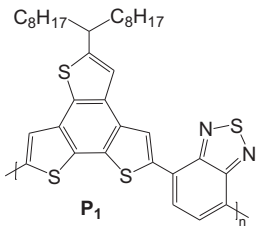


Fig. 11. Copolymer **P1** based on **bbb-BTT-2-**BTZ monomer.

An efficient strategy to broaden the absorption spectra of the light-harvesting materials is the incorporation of several different chromophores into one polymeric donor material [6b]. In this perspective, Nielsen reported a highly successful improving of OPV efficiency by randomly copolymerizing **bbb-BTT-2** and **DPP** with a third monomer M3 (Fig. 12) [48].

Beside the good polymer solubility and processability, the result was to expand the optical absorption and improve the light-harvesting properties.

The terpolymers gave highly efficient OPV devices displaying high currents. BTZ-containing terpolymer **P2** displayed a PCE of 5.14%, nearly the double of the parent alternating copolymer **bbb-BTT-2–DPP**.

A new semiconducting **bbb-BTT-2-BTZ** (Fig. 13) copolymer, having a broad-band gap and high open-circuit voltage, was synthesised by Yang [49].

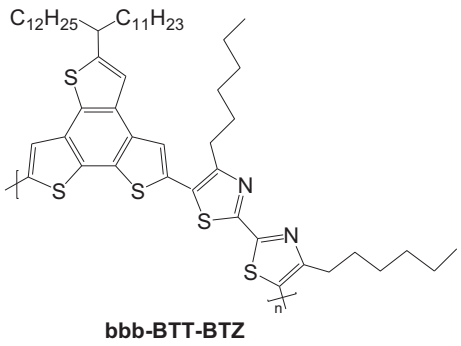
The photovoltaic device based on the **bbb-BTT-2-BTZ** copolymer/PC71BM photoactive layer showed a PCE of 2.49%. The morphology of the blend film was significantly optimized after treatment with 1,8-diiodooctane as additive, and the PCE reached 5.06%.

Modulation of the nature and the content of the third monomer enabled a fine-tuning of the frontier energy levels, an important optimization of the optical absorption [50].

The free 5- and 6-positions of the BTZ moiety have demonstrated to be suitable for attaching electron-donating and electron-withdrawing substituents in order to modulate the energy of the frontier-orbital energies in the copolymers, as well as to increase their solubility, with the aim to improve the performance of fullerene-based solar cells (Fig. 14).

In general, the introduction on BTZ of different substituents with increasing acceptor strength stabilizes both LUMO and HOMO energies in the order OR (O2BT) > H (BTZ) > F (F2BT), affording an increase in open-circuit voltage, while other parameters are largely unaffected in cases where there is sufficient energetic offset for electron transfer to the fullerene. Furthermore, Nielsen found that substituting a cyclic imide in 5–6 positions, thus obtaining the 2,1,3-benzothiadiazole-5,6-dicarboxylic imide (BTI), resulted in an electron-accepting unit stronger than F2BT and the concomitant lowering of the HOMO and LUMO energy levels.

Co-polymerization of dithienyl-BTI was carried out with **bbb-BTT-2**, a co-monomer with well-known charge transport properties (Fig. 15). The alkyl chain, that is required to induce solubility and processability, was introduced in both the electron-rich **bbb-BTT-2** and the electron-deficient BTI monomers. This allowed for the optimization of OPV device performance realized without needs of solvent additives and solvent/thermal-annealing steps. The photovoltaic properties of **BBTI-1** and **BBTI-2** were examined



bbb-BTT-BTZ

Fig. 13. Copolymer **bbb-BTT-BTZ**.

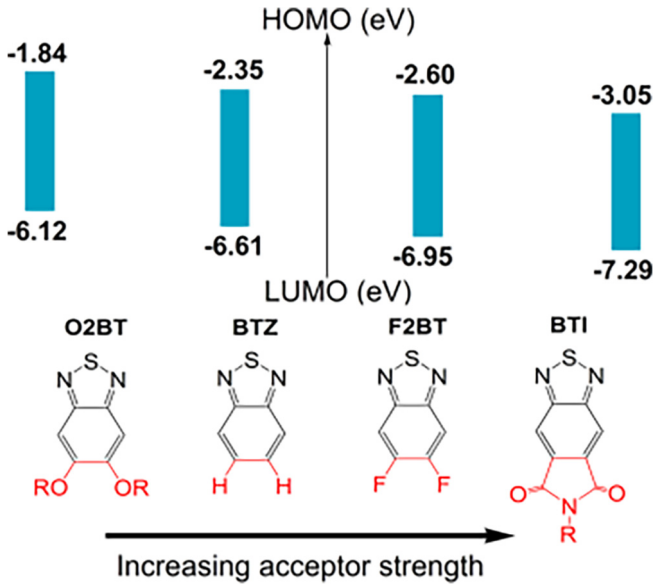
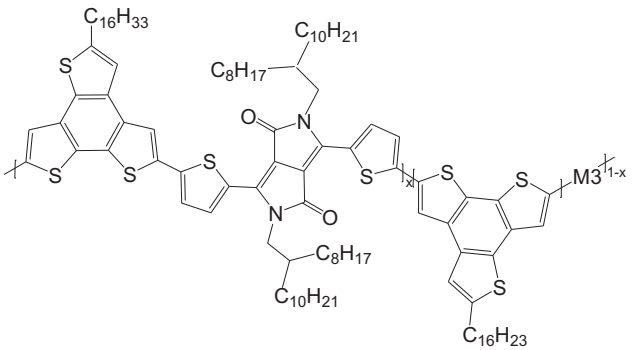


Fig. 14. Chemical modifications of BTZ system positions with theoretical HOMO and LUMO energy levels (Gaussian at the B3LYP/6–31G* level of theory).

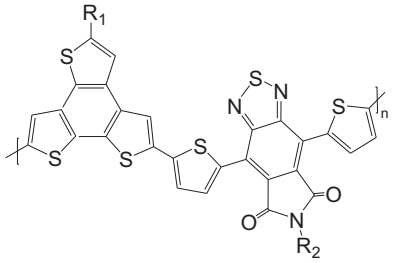
in an OPV device with $PC_{71}BM$ as the electron acceptor material, affording solar cells with PCE reaching 8.3%.

With the same strategy, two donor-acceptor copolymers containing BTZ and 2,5-dibromo-8-dodecanoyl- **bbb-BTT-2** (**P6**) or 2,8-dibromo-5-dodecanoyl- **bbb-BTT-2** (**P7**) acceptor units with thiophene donor (Fig. 16) were synthesised by Keshtov and Sharma [51].



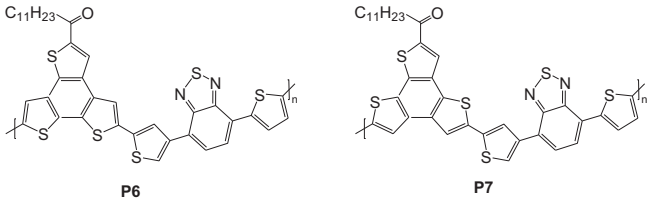
P2: M3 = BTZ, x = 0.75
P3: M3 = C_8-TPD, x = 0.75
P4: M3 = C_8C_8-**bbb-BTT-2**, x = 0.75
P5: M3 = C_8C_8-**bbb-BTT-2**, x = 0.50

Fig. 12. Copolymers **P2-P5** based on **bbb-BTT-2-DPP** monomer. DPP = diketopyrrolopyrrole, BTZ = 2,1,3-benzothiadiazole, C_8-TPD = *N*-octylthienopyrrolodione, C_8C_8 = 1-octylnonyl.



BBTI-1: R_1 = C16, R_2 = C10C14
BBTI-2: R_1 = C9C10, R_2 = C10C14

Fig. 15. Copolymers of dithienyl-**BBTI-1** and **bbb-BBTI-2** monomers.



P6 **P7**

Fig. 16. Copolymers of BTZ and 2,5-dibromo-8-dodecanoyl-**bbb-BTT-2** (**P6**) or 2,8-dibromo-5-dodecanoyl- **bbb-BTT-2** (**P7**) with thiophene.

Their HOMO and LUMO energy levels indicated that there is sufficient LUMO offset with $PC_{71}BM$ for efficient exciton dissociation, and deeper HOMO levels to ensure high open-circuit voltage for the optimized BHJ solar cells, showing PCE of 7.19% (**P6**) and 6.34% (**P7**).

OFET devices

In parallel to its use as donor unit for in OPV devices, **bbb-BTT-2** moiety was firstly developed by Nielsen for OFET applications [24b]. Co-polymerization of **bbb-BTT-2** bearing a branched C_8C_8 alkyl chain, with thiophene or thieno[3,2-*b*]thiophene units as co-monomers, gave highly ordered polymers, namely **BTT-T** and **BTT-TT** respectively. Both polymers displayed good charge carrier mobility when employed as semiconducting materials in OFETs, despite polymerization gave rise low molecular weights due to strong aggregation effects and limited solubility. In addition, the co-monomer played a crucial role in determining the backbone conformation, the interchain interactions, the polymer solubility and the charge carrier mobility.

In fact, the minimum-energy conformations of **BTT-T** and **BTT-TT** tetramers, obtained by DFT calculations, revealed significant differences between the two systems as depicted in Fig. 17. The intrachain separation of the alkyl-bearing BTT unit increased as the size of the co-monomer raised from thiophene to thieno[3,2-*b*]thiophene, causing a decrease of polymer solubility.

Moreover, the backbone of **BTT-T** resulted slightly curved with all alkyl groups facing the same side of the backbone, whereas **BTT-TT** displayed a planar zig-zag conformation and long range linearity, with adjacent alkyl groups on opposite sides of the backbone.

These factors support the higher-molecular-weight chain growth during the polymerization of **BTT-T**, which was more curved, less structured and, consequently, more soluble compared to **BTT-TT**. The molecular weight for **BTT-T** was M_n = 16.6 kDa (PDI = 2.90), whereas the polymerization was stopped at a low degree of polymerization (M_n = 6.2 kDa, PDI = 2.11) as the further increase of the molecular weight gave insoluble polymers.

The polymer films of **BTT-T** and **BTT-TT** showed hole-mobility of 0.24 and 0.025 $cm^2\ V^{-1}\ s^{-1}$, respectively The one-order-of-magnitude-larger charge carrier mobility of **BTT-T** was attributed to the threefold increase in molecular weight. Nevertheless, the mobility of **BTT-TT** is unexpectedly high for a polydisperse oligomer with about ten units, indicating that even the short chains of **BTT-TT** are able to transport charge in the solid state. Both **BTT-T** and **BTT-TT** polymers displayed good transfer and output charac-

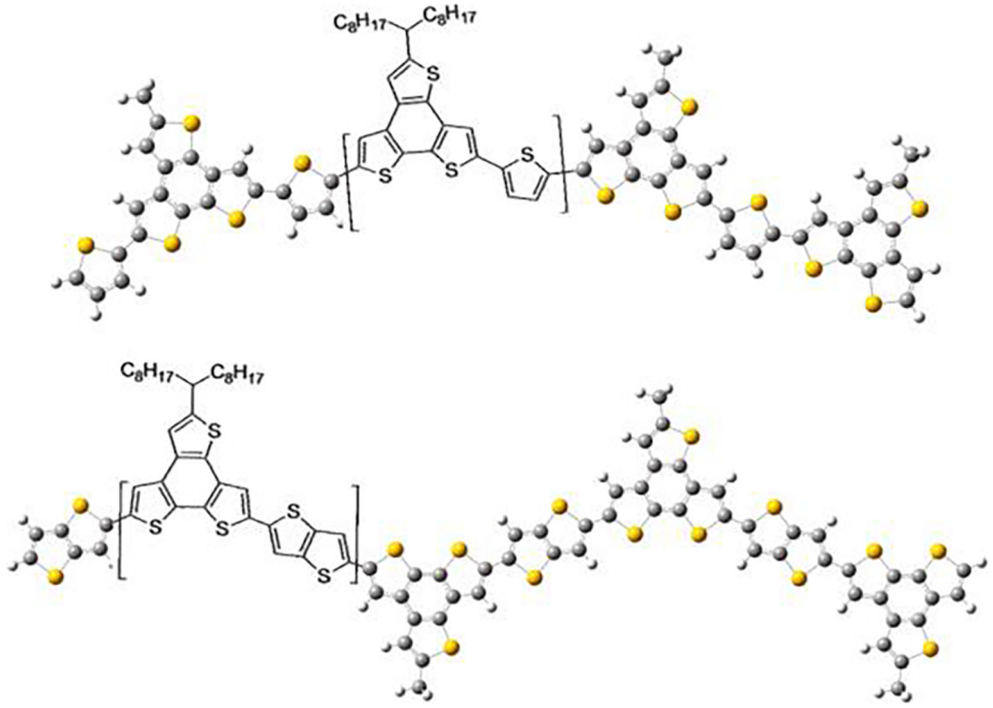


Fig. 17. Minimum-energy conformations of tetramers of **BTT-T** (top) and **BTT-TT** (bottom) Gaussian-optimized at the B3LYP/6-31G* level (for simplicity, the polymer structures are drawn in a regioregular fashion with respect to the position of the asymmetric alkyl-bearing thiophene unit). Reprinted with permission from Schroeder, B. C.; Nielsen, B. C.; Kim, Y. J.; Smith, J.; Huang, Z.; Durrant, J.; Watkins, S. E.; Song, K.; Anthopoulos, T. D.; McCulloch, I. *Chem. Mater.* **2011**, *23*, 4025–4031. Copyright (2011) by the American Chemical Society.

teristics, and the low-lying HOMO levels support good stability, an important feature for potential commercialization, although making hole-injection more difficult.

Overcoming solubility and processability difficulties, by side chain optimization, **BTT-T** is promising for OFET applications.

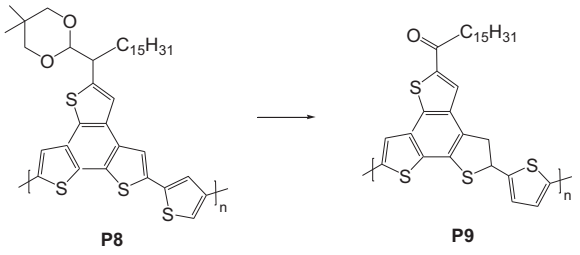
In this perspective, it was shown that ketalization of acyl-functionalized **bbb-BTT-2**-containing polymer (**P8**) can significantly increase the solubility [21]. A successive cleavage by a thermal annealing process was realized in the solid state, easily converting **P8** to the corresponding ketone-functionalized **BTT-T** copolymer (**P9**) (Scheme 21).

The latter exhibited a much more ordered solid state packing and a greatly increased hole-mobility from 7.0×10^{-4} to 1.0×10^{-2} cm^2 V^{-1} s^{-1}) [52].

In order to investigate the effect of the side-chain nature, Zhang [5a] synthesised a series of **BDT** and **bbb-BTT-2**-based conjugated polymers (**P10**–**P13**), with the conjugated alkyl-thiophene on **BDT** and alkyl or acyl side chains on **bbb-BTT-2** (**P10** and **P11**), alkyloxy on **BDT** and alkyl or acyl side chains on **bbb-BTT-2** (**P12** and **P13**) (Fig. 18). The nature of side chains strongly influenced the thermal and electronic features of the polymers. The conjugated-side chain raised the thermal stability while the acyl-side chain lowered HOMO-LUMO energy levels.

Even the device performance of the obtained thin-film transistors was sensitive to the side chains. For **P10** a hole-mobility of 1.7×10^{-3} cm^2 V^{-1} s^{-1} was obtained, one order of magnitude higher of than those of **P12** and **P13**-based devices.

Nielsen [53] incorporated the **bbb-BTT-2** planar unit into four different donor polymers (Fig. 19). The different nature and positioning of the side chains along the polymer backbone influenced the HOMO-LUMO energy, the solubility of the polymers and solid-state packing. Both **BTT**- and **COBTT**-type monomers were obtained with either 4,4′-dihexyl-2,2′-bithiophene, which introduces a tail-to-tail (tt) between two adjacent thiophene rings, or with 3,3′-dihexyl-2,2′-bithiophene, causing a head-to-head (hh).



Scheme 21. Thermal annealing of **P8** to **P9**.

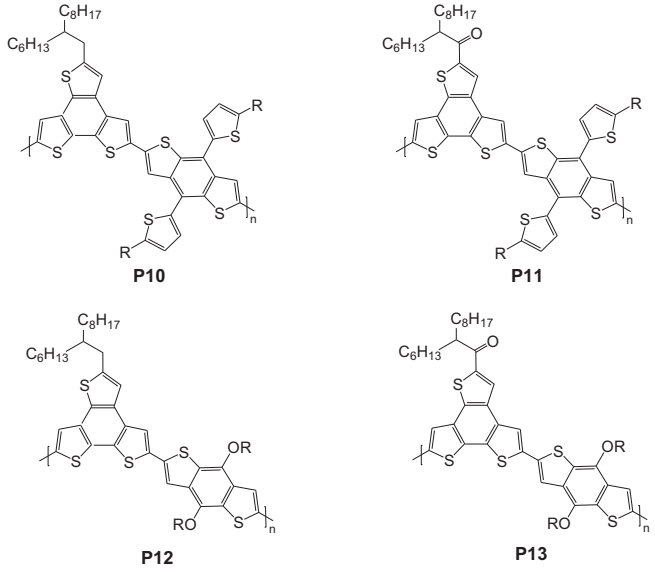


Fig. 18. A series of **BDT** and **bbb-BTT-2**-based conjugated polymers.

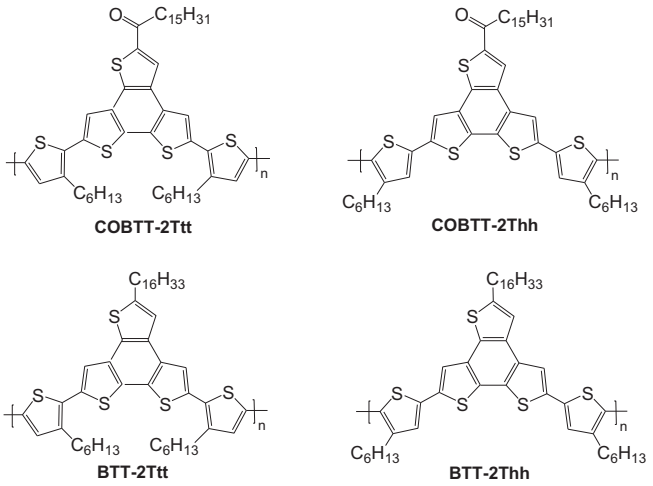


Fig. 19. Tail-to-tail (**COBTT-2Ttt** and **BTT-2Ttt**) and head-to-head (**COBTT-2Thh** and **BTT-2Thh**) polymers.

Both **BTT**- and **COBTT**-type monomers were obtained with either 4,4′-dihexyl-2,2′-bithiophene, which introduces a tail-to-tail (tt) between two adjacent thiophene rings, or with 3,3′-dihexyl-2,2′-bithiophene, causing a head-to-head (hh). Linear hexadecyl (**BTT-2Ttt** and **BTT-2Thh**) and hexadecanoyl (**COBTT-2Ttt** and **COBTT-2Thh**) side chains favored intermolecular packing of the **BTT** cores. The electron withdrawing acyl side chain perturbs the electronic distribution of the **BTT** core compared to the alkyl side chain. The positioning and the steric hindrance caused by the addition of alkyl chains determined solubility and molecular packing, tuning the processability as well.

The head-head coupling in **BTT-2Thh** polymer induced a backbone twist, which reduced the conjugation length and increased the optical band-gap. The tail-to-tail polymer **BTT-2Ttt** displayed a higher lying HOMO energy level while the LUMO energy level was not affected by the alkyl chain positioning, resulting in a band-gap than smaller than that of the **BTT-2Thh** polymer. The introduction of the carbonyl groups lowered the LUMO energy levels of both **COBTT** polymers compared to the **BTT** polymers, but the overall band-gaps were scarcely affected. In addition, the presence of carbonyl groups induced interchain aggregation reducing the twisting, therefore lowering the HOMO energy levels less than in the case of the head-to-head coupled **BTT** copolymers.

The steric hindrance along the polymer backbone was reduced in **BTT-2Ttt** and **COBTT-2Ttt** leading to strong interchain aggregation in both solution and solid state and highly ordered thin film. The enhanced order of **BTT-2Ttt** and **COBTT-2Ttt**, was supposed to be responsible of the higher hole-mobility in thin film transistors (0.04 and 0.01 cm^2 V^{-1} s^{-1}, respectively) compared to the head-to-head coupled polymers **BTT-2Thh** and **COBTT-2Thh** (1.6×10^{-5} and cm^2 V^{-1} s^{-1}, respectively). In addition, introduction of the carbonyl groups on the conjugated backbone increased the ambient stability of the polymers.

bbc-BTT-3 devices

Applications of **bbc-BTT-3-**core have been actually reported only in OFET devices [5b,54]. This donor unit possesses a higher

HOMO level than all of the other **BTT** isomers and is a potential donor component for D-A copolymers [14].

After the synthesis of **bbc-BTT-3** as a new member of the **BTT** family, Müllen reported the preparation of the first D-A copolymers, **P14** and **P15** (Fig. 20) [54]. The donor monomer **bbc-BTT-3** was coupled with the strong acceptors BTZ (**P14**) and bis(5-thienyl)-BTZ (**P15**). The single-crystal structure of the alkyl-substituted **bbc-BTT-3** showed that the solubilizing dodecyl chains lie nearly in the same plane as the conjugated core and stretch out along an angle of around 55° with respect to the *C*2 symmetry axis.

In the corresponding polymers, the location of the alkyl chains, planar with the polymer backbone, reduced the π-staking between the polymer chains (0.35 nm for **P14** and 0.37 nm for for **P15**) much more than in other polymers with alkyl chains out of the main chains. Calculations showed that the **P14** backbone is more curved than that of **P15**, contributing to a better solubility of the former. In addition, insertion of two thiophene units in **P15** considerably modified the chain conformation, the supermolecular organization, the film microstructure and, consequently, the charge carrier transport (Fig. 21).

The onset of the **P14** and **P15** thin-film absorptions indicated optical band-gaps of 1.35 and 1.53 eV, narrower values compared with that of the D – A copolymer **P1** obtained with **bbb-BTT-2** and BTZ (Fig. 11), demonstrating the stronger electron-donating nature of **bbc-BTT-3** donor unit.

Finally, despite a supramolecular organization found in the bulk with a good π-stacking distance of only 0.35 nm, **P14** did not show any field-effect response because of the pronounced disorder in the thin film. In contrast, **P15** exhibited a hole-mobility of 0.04 $cm^2 V^{-1} s^{-1}$, owing to the well-ordered film and a supramolecular organization into lamellar structures with a π-stacking distance of 0.37 nm.

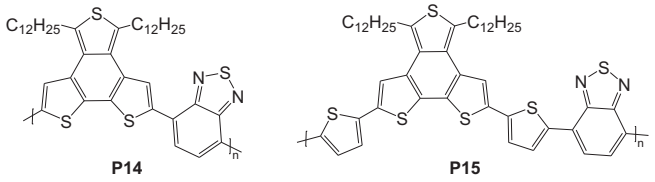


Fig. 20. Donor-acceptor copolymer of **bbc-BTT-2**.

This is the first example of **BTT**-based D – A copolymers exhibiting distinguishing supramolecular organization and sensible field-effect behaviour.

In order to improve the charge transport within **BTT**-containing polymers, BTZ of **P15** was replaced with DPP [5b], an acceptor unit able to reinforce the intermolecular interaction and to improve the π–stacking between polymer chains [3a,55], preparing the polymers **P16** and **P17** (Fig. 22).

The new donor–acceptor **bbc-BTT-3-DPP** copolymers, differing for the presence (**P16**) or absence (**P17**) of alkyl side chains at the **bbc-BTT-3** unit, exhibited a remarkable modification in packing order, thin-film arrangement and charge carrier transport.

Because of the stronger donor-acceptor interaction, changing BTZ with DPP in **P16** led to a considerable red-shift of the absorption band and a decreased optical band-gap. However, the steric hindrance between alkyl chains onto the DPP and **bbc-BTT-3** units resulted in twisting the polymer backbone and decreasing the order, thus reducing the hole-mobility of **P17** (0.007 $cm^2 V^{-1} s^{-1}$). The removal of alkyl chains on **bbc-BTT-3** unit excluded the steric interactions, changed the arrangement of the polymers on the surface and improved the OFET performance, with a hole-mobility (0.2 $cm^2 V^{-1} s^{-1}$) higher than those of both **P14** and **P15**, making the **bbc-BTT-3**-based polymers promising candidates in OFET application.

BTT-based materials in perovskite solar cells

Since the first introduction in 2009 of organic–inorganic hybrid methylammonium lead halide ($MAPbX_3$) perovskites as active materials for PV applications [56], the PCE of perovskite-based solar cells (PSCs) have been extremely improved within a few years from the 14% to a recently certified 24.2% values, which is the fastest growing photovoltaic technology in history [57,58].

The best lifetime obtained for perovskite solar cells is around 1 year (10,000 h) but the PCE is only 12% [59]. To achieve an efficiency of 20%, the best stability is only 1000 h [60]. More than 90% of the commercialised photovoltaic cells is silicon-based because it provides an average efficiency of 21%, lifetime of more than 25 years and low cost [59].

Taking into account that the photovoltaic market is still dominated by silicon-based solar cells, transforming about 26% sunlight

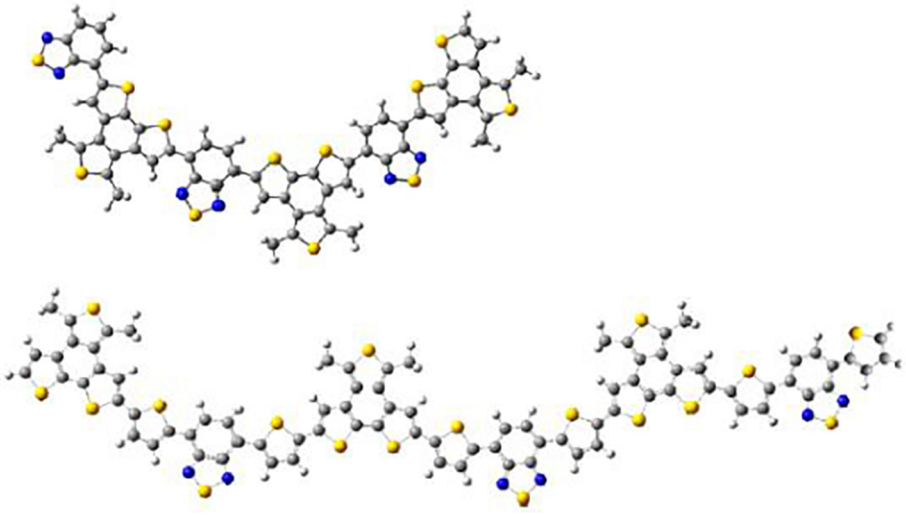


Fig. 21. Minimum-energy conformations of methyl-substituted trimers of (top) **P14** and (bottom) **P15** optimized at the B3LYP/6-31G* level. Reprinted with permission from Guo, X.; Puniredd, S. R.; Baumgarten, M.; Pisula,W.; Müllen, K. *J. Am. Chem. Soc.* **2012**, *134*, 8404–8407. Copyright (2012) by the American Chemical Society.

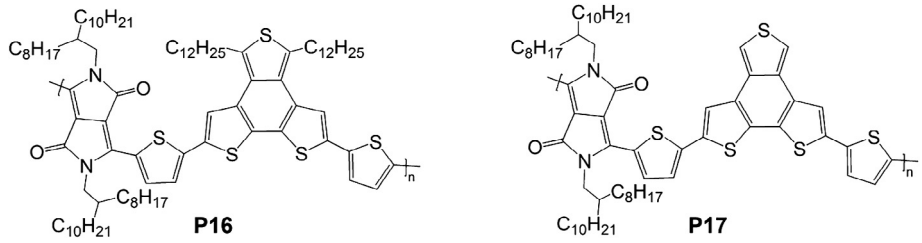


Fig. 22. Donor-acceptor **bbc-BTT-3-DPP** copolymers.

into electricity for crystalline silicon and 22% for microcrystalline silicon devices, the research on PSCs have experienced a huge scientific interest for photovoltaic applications [57,61].

In view to improve the hole-transporting ability of **bbb-BTT-1** devices, Nazeeruddin and Martín prepared three star-shaped small molecule by crosslinking **bbb-BTT-1** core with different triphenylamine based ligands (Fig. 22): **BTT-**1 with *p*-methoxydiphenylamine (OMeDPA), **BTT-2** with *p*-methoxydiphenylamine-substituted carbazole (OMeDPAC), and **BTT-3** with *p*-methoxytriphenylamine (OMeTPA) (Fig. 23) [31].

These compounds displayed efficient hole-transporting properties and, when implemented in PSCs, exhibited excellent performances comparable to the state-of-the-art PSCs. PCE up to 16% and 17% were obtained for **BTT-1** and **BTT-2**, respectively, and 18.2% for **BTT-3**. The last value is comparable to the reference 2,2,7,7-tetrakis(N,*N*-di-*p*-methoxyphenylamine)-9,9-spirobifluorene (spiroOMeTAD), the most commonly used hole-transporting material, and among the highest PCE values observed for PSCs using a small molecule so far.

Theoretical DFT calculations [62] showed that bulky groups, such as OMeDPA and OMeDPAC, give rise to highly crowd molecular structures. In contrast, OMeTPA groups led to an almost planar structure more suitable for a stacking aggregation, desirable for more efficient charge transport and performance of the OPV device.

In 2017, the same authors [63] described the synthesis, characterization and photovoltaic performance of **BTT-4** and **BTT-5** molecules based on the isomeric **bbb-BTT-2** and **bbc-BTT-3** bearing three and four OMeTPAs, respectively (Fig. 24). The different arrangement of the sulphur atoms provided hole-transporting materials with different properties.

The HOMO/LUMO energy levels calculated for the OMeTPA pendant groups, the **BTT** cores, the **BTT**-based hole- transporting materials and the archetypical material for PSCs spiroOMeTAD are displayed in Fig. 25.

The frontier-orbital energies of the **BTT** derivatives reflected their structural changes. In fact, the HOMO/LUMO is significantly destabilized/stabilized in passing from **bbb-BTT-1** (2−5.79/−0.89 eV) to **bbb-BTT-2** (−5.67/−1.22 eV) and to **bbc-BTT-3** (−5.36/−1.56 eV). This destabilization/stabilization is due to the more effective conjugation of the core, especially for **bbc-BTT-3**, giving rise to a decrease of the HOMO–LUMO gap. The HOMOs of **BTT-3**, **BTT-4** and **BTT-5** are destabilized with respect to the corresponding **BTT** cores, as the result of the antibonding interaction with the OMeTPA arms, and undergo a destabilization from **BTT-3** (−4.73 eV) to **BTT-4** (−4.61 eV) and **BTT-5** (−4.50 eV), approaching the HOMO level calculated for spiroOMeTAD (−4.44 eV). In addition, these materials are polarized and a significant charge transfer takes place from the peripheral OMeTPA groups to the central **BTT** core, more pronounced for **BTT-5** due to its four-armed structure.

It appeared that the **BTT**-based molecules are good electron donors, and their HOMO energy levels are suitably aligned with the valence band of the perovskite, suggesting an efficient hole-injection from the **BTT** materials.

In addition, **BTT-4** and **BTT-5** demonstrated good thermal stability of up to 430 °C. Remarkably, **BTT-4** and **BTT-5** showed extraordinary PCE values of 19% and 18.2%, respectively, exceeding the efficiency exhibited by **BTT-3** (17.2%) and the commonly used spiroOMeTAD (18.9%), even approaching the performances of silicon-based solar cells. The author assumed that the *cis* arrangement of the sulfur atoms might benefit the interaction with the perovskite material.

Very recently, the profitable approach to PSCs, was exploited by Singh [64] to enhance the performance of **bbb-BTT-1** and DPP-based molecules (Fig. 26).

These star-shaped small molecules have been synthesised and tested as hole-transporting material in PSCs. The fine-tuning of the molecular structures allowed to achieve a PCE up to 14.13% for **BTT(DPP-Th)3-EH** over those for **BTT(DPP)3-C8** (8.65%) and **BTT(DPP)3**-EH (8.39%).

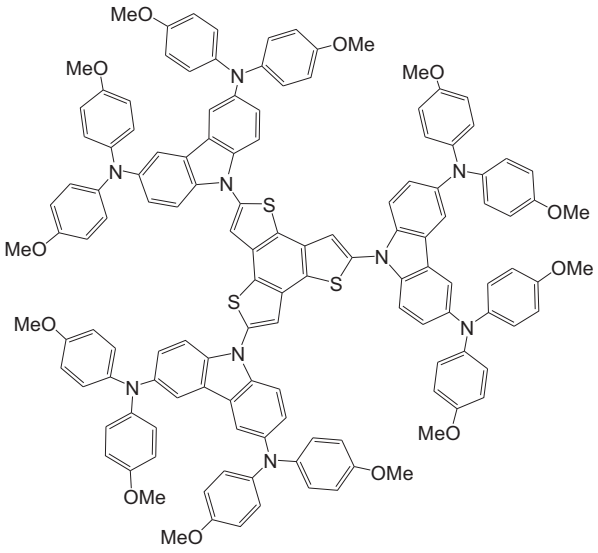
Conclusion and outlook

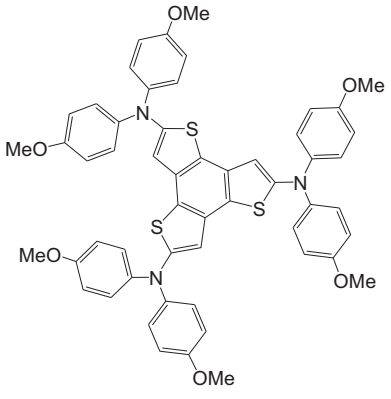
In this digest, we have reported an overview of the advances over the last sixteen years in the synthesis and applications of benzotrithiophene (**BTT**) isomers as π-cores for organic electronic materials. These studies demonstrated that **BTT**s possess significant potential as semiconductors for fabrications of electronic devices such as solar cells, field-effect transistors, electrochromic materials, high-area capacitors and charge carrier discotic liquid crystals. The impressive results, obtained in a relative short time, indicate that **BTT**s are adaptable and useful building blocks for the design of high-performance and stable devices.

BTTs possesse rigid and planar conjugated structures which allow for finely tuning the molecular energy levels and optical band-gaps as well as high hole-mobility. The third fused thiophene extends the aromatic core favoring intermolecular π-stacking and charge transport. It appears that the third thiophene unit of **BTT**s is preferable to a benzene unit. For instance, compared to the well-known benzodithiophene (**BDT),** one of the most promising photovoltaic materials, DFT calculations predicted for **bbb-BTT-2** similar donor strength to the **BTT**s. The similar open-circuit voltages confirm the comparable HOMO energy levels for the two systems, reflecting their analogous donor strengths. However, there are evidences that the larger **BTTs** unit have an advantageous influence on the charge transport in an OPV device.

Besides, the fine-tuning of the frontiers orbital energies, the design of these organic material has considered the variations in the structure of the molecular backbone molecular shape and geometry, the side chain effects, the copolymerization with different co-monomers, the molecular-weight characteristics, the light-harvesting properties, the solubility and the processability.

In particular, the three-dimensional functionalization of **BTT**s with side groups represents a feasible and efficient method to increase the electronic performance of the conjugated materials, obtaining, for instance, PCE value and hole-mobility up to 9.43% and 0.24 $cm^2\ V^{-1}\ s^{-1}$ in OPV and OFET devices, respectively.





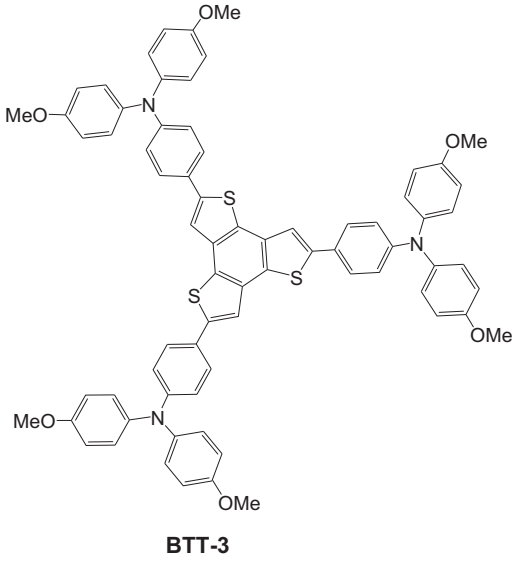
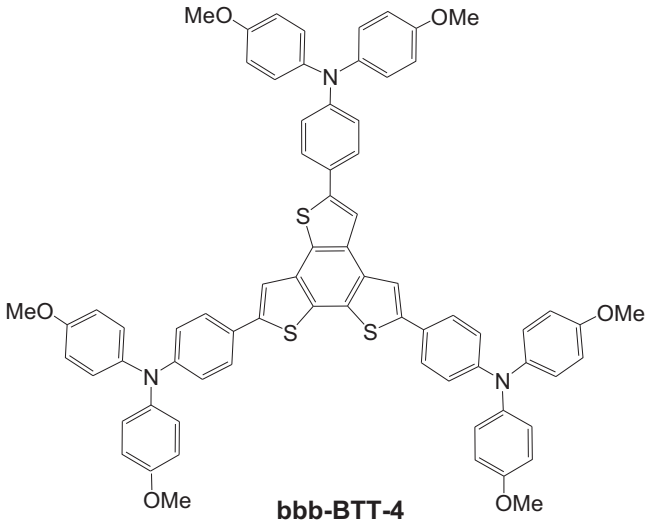


Fig. 23. Star-shaped **BTT-1**, **BTT-2** and **BTT-3** with **bbb-BTT-1** core.

Finally, the implementation of some **BTT**-based small molecules in PSCs allowed for achieving excellent performances comparable to the state-of-the-art perovskites based devices up to PCE of



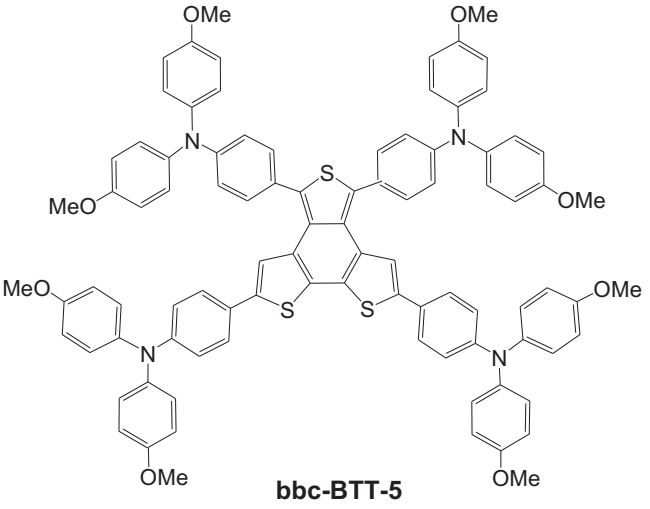


Fig. 24. BTT-4 and **BTT-5** molecules based on the isomeric **bbb-BTT-2** and **bbc-BTT-3** bearing three and four OMeTPAs.

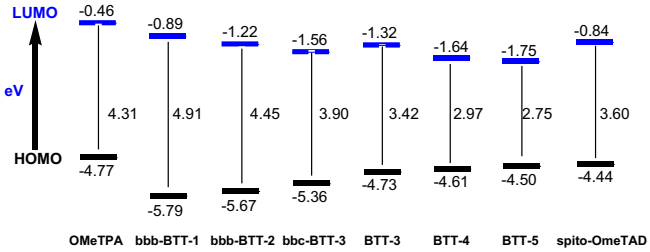
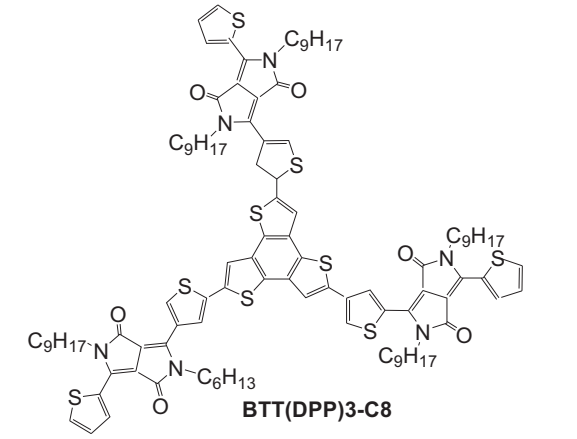
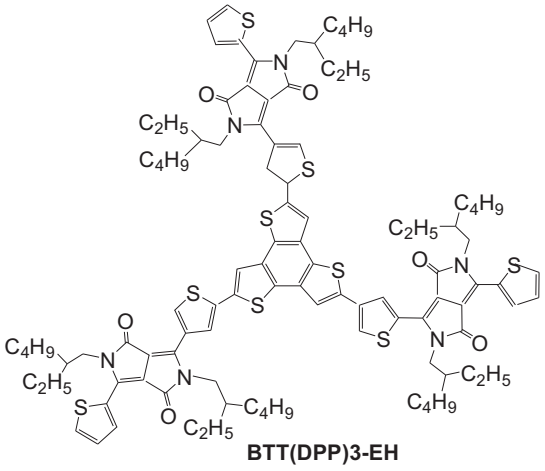


Fig. 25. Energy level of the frontier molecular orbitals (Gaussian at the B3LYP/6–31G* level of theory in CH_2Cl_2).

19%, even exceeding the efficiency exhibited by the commonly used spiroOMeTAD and approaching the performances of silicon-based solar cells.

The rapid improvement in synthetic ability has made available a wide set of tools for constructing new polymer networks but a number of challenges also need to be pursued. An important task is the processability, i.e. while linear polymers are seldom soluble in organic solvents, networks are not easily dissolved in organic media. This opens the query of processing to the best these





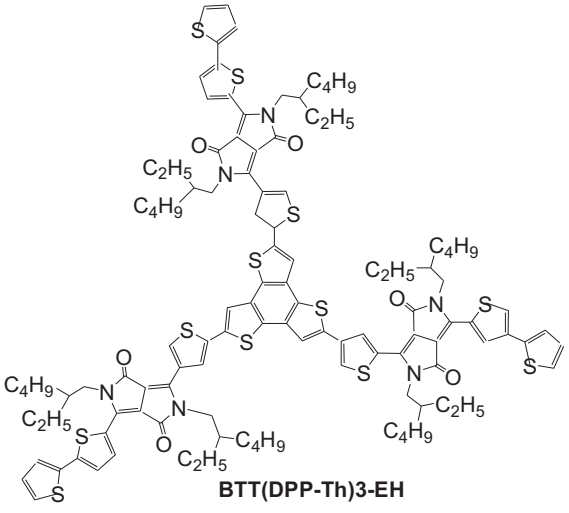


Fig. 26. bbb-BTT-1 and DPP-based molecules.

materials into functional devices. Although in some case solution-processable hyperbranched conjugated polymers are obtained, the absolute efficiencies are modest.

Furthermore, among the main key requirements when converting organic-inorganic electronic devices from laboratory to commerce (low cost, high power conversion efficiency and long lifetime), high stability of **BTT**-based materials has occasionally been studied. Therefore, evaluating the effects of the environmental (moisture and air stability) and intrinsic factors (hygroscopicity, thermal instability and ion migration) on long-term stability of high-efficiency materials is required.

Acknowledgement

Financial support by the University of Padova through the grant PRAT 2014 action (2015K7FZLH) is acknowledged.

References

[1] (a) L. Lu, T. Zheng, Q. Wu, A.M. Schneider, D. Zhao, L.R. Yu, Chem. Rev. 115 (2015) 12666–12731;
(b) L. Dou, Y. Liu, Z. Hong, G. Li, Y. Yang, Chem. Rev. 115 (2015) 12633–12665;
(c) C. Wang, H. Dong, W. Hu, Y. Liu, D. Zhu, Chem. Rev. 112 (2012) 2208–2267.
[2] A. Mishra, C.-Q. Ma, P. Bäuerle, Chem. Rev. 109 (2009) 1141–1276.
[3] (a) H. Bronstein, Z. Chen, R.S. Ashraf, W. Zhang, J. Du, J.R. Durrant, P.S. Tuladhar, K. Song, S.E. Watkins, Y. Geerts, M.M. Wienk, R.A.J. Janssen, T. Anthopoulos, H. Sirringhaus, M. Heeney, I. McCulloch, J. Am. Chem. Soc. 133 (2011) 3272–3275;
(b) Y. Zou, A. Najari, P. Berrouard, S. Beaupré, B.R. Aïch, Y. Tao, M. Leclerc, J. Am. Chem. Soc. 132 (2010) 5330–5331;
(c) E. Zhou, M. Nakamura, T. Nishizawa, Y. Zhang, Q. Wei, K. Tajima, C. Yang, K. Hashimoto, Macromolecules 41 (2008) 8302–8305;
(d) R. De Bettignies, Y. Nicolas, P. Blanchard, E. Levillain, J.M. Nunzi, Roncali, J. Adv. Mater. 15 (2003) 1939–1943.
[4] (a) M.X. Chen, E. Perzon, N. Robisson, S.K.M. Jönsson, M.R. Andersson, M. Fahlman, M. Berggren, Synth. Met. 146 (2004) 233–236;
(b) M. Mazzeo, V. Vitale, F. Della Sala, D. Pisignano, M. Anni, G. Barbarella, L. Favaretto, A. Zanelli, R. Cingolani, G. Gigli, Adv. Mater. 15 (2003) 2060–2063.
[5] (a) G. Zhang, M. Zhu, J. Guo, J. Ma, X. Wang, H. Lu, L. Qiu, Org. Electr. 15 (2014) 2608–2615;
(b) X. Guo, S.R. Puniredd, M. Baumgarten, W. Pisula, K. Müllen, Adv. Mater. 25 (2013) 5467–5472;
(c) D. Patra, T.-Y. Huang, C.-C. Chiang, R.O.V. Maturana, C.-W. Pao, K.-C. Ho, K.-H. Wei, C.-W. Chu, ACS Appl. Mater. Interfaces 5 (2013) 9494–9500;
(d) T. Yamamoto, K. Takimiya, J. Am. Chem. Soc. 129 (2007) 2224–2225;
(e) K. Takimiya, Y. Kunugi, Y. Toyoshima, T. Otsubo, J. Am. Chem. Soc. 127 (2005) 3605–3612.
[6] (a) T. Taerum, O. Lukoyanova, R.G. Wylie, D.F. Perepichka, Org. Lett. 11 (2009) 3230–3233;
(b) P.M. Beaujuge, S. Ellinger, J.R. Reynolds, Nat. Mater. 7 (2008) 795–799.
[7] H. Yao, L. Ye, H. Zhang, S. Li, S. Zhang, J. Hou, Chem. Rev. 116 (2016) 7397–7457.
[8] (a) Y. Wu, Z. Li, W. Ma, Y. Huang, L. Huo, X. Guo, M. Zhang, H. Ade, J. Hou, Adv. Mater. 25 (2013) 3449–3455;
(b) W. Lee, G.-H. Kim, S.-J. Ko, S. Yum, S. Hwang, S. Cho, Y.-H. Shin, J.Y. Kim, H. Y. Woo, Macromolecules 47 (2014) 1604–1612;
(c) S.-C. Lan, P.-A. Yang, M.-J. Zhu, C.-M. Yu, J.-M. Jiang, K.-H. Wei, Polym. Chem. 4 (2013) 1132–1140.
[9] (a) J.-M. Jiang, H.-K. Lin, Y.-C. Lin, H.-C. Chen, S.-C. Lan, C.-K. Chang, K.-H. Wei, Macromolecules 47 (2014) 70–78;
(b) L. Ye, S. Zhang, L. Huo, M. Zhang, J. Hou, Acc. Chem. Res. 47 (2014) 1595–1603;
(c) T. Qin, W. Zajaczkowski, W. Pisula, M. Baumgarten, M. Chen, M. Gao, G. Wilson, C.D. Easton, K. Müllen, S.E. Watkins, J. Am. Chem. Soc. 136 (2014) 6049–6055;
(d) C. Cui, W.-Y. Wong, Y. Li, Energy Environ. Sci. 7 (2014) 2276–2284.
[10] J.K. Park, J. Jo, J.H. Seo, J.S. Moon, Y.D. Park, K. Lee, A.J. Heeger, G.C. Bazan, Adv. Mater. 23 (2011) 2430–2435.
[11] (a) W. Li, L. Yang, J.R. Tumbleston, L. Yan, H. Ade, W. You, Adv. Mater. 26 (2014) 4456–4462;
(b) J.A. Bartelt, J.D. Douglas, W.R. El Mateker, A.C.J. Labban, Toney Tassone, M. F. Fr|chet, J.M.J. Beaujuge, P.M. McGehee, Adv. Energy Mater. 4 (2014) 1301733–1301744.
[12] (a) R. Proetzsch, D. Bieniek, F. Korte, Tetrahedron Lett. (1972) 543–544;
(b) N. Jayasuriya, J. Kagan, J. Org. Chem. 54 (1989) 4203–4205;
(c) T. Kashiki, S. Shinamura, M. Kohara, E. Miyazaki, K. Takimiya, M. Ikeda, H. Kuwabara, Org. Lett. 11 (2009) 2473–2475;
(d) T. Kashiki, M. Kohara, I. Osaka, E. Miyazaki, K. Takimiya, J. Org. Chem. 76 (2011) 4061–4070.
[13] (a) H. Hart, M. Sasaoka, J. Am. Chem. Soc. 100 (1978) 4326–4327;
(b) A. Patra, Y.H. Wijsboom, L.J.W. Shimon, M. Bendikov, Angew. Chem., Int. Ed. 46 (2007) 8814–8818.
[14] X. Guo, S. Wang, V. Enkelmann, M. Baumgarten, K. Müllen, Org. Lett. 13 (2011) 6062–6065.
[15] Y. Nicolas, P. Blanchard, E. Levillain, M. Allain, N. Mercier, J. Roncali, Org. Lett. 6 (2004) 273–276.
[16] R. Sanz, M.P. Castroviejo, V. Guilarte, A. Pérez, F.J. Fãnanás, J. Org. Chem. 72 (2007) 5113–5118.
[17] L.L. Sun, C.L. Deng, R.Y. Tang, X.G. Zhang, J. Org. Chem. 76 (2011) 7546–7550.
[18] (a) S. Rossi, A. Bisello, R. Cardena, L. Orian, S. Santi, Eur. J. Org. Chem. (2017) 5966–5974;
(b) S. Rossi, A. Bisello, R. Cardena, S. Santi, Organometallics 37 (2018) 4242–4249;
(c) A. Donoli, A. Bisello, R. Cardena, C. Prinzivalli, S. Santi, Organometallics 32 (2013) 1029–1036;

(d) A. Donoli, A. Bisello, R. Cardena, F. Benetollo, A. Ceccon, S. Santi, Organometallics 30 (2011) 1116–1121.
[19] (a) I.P. Beletskaya, V.P. Ananikov, Chem. Rev. 111 (2011) 1596–1636;
(b) I. Nakamura, T. Sato, Y. Yamamoto, Angew. Chem. Int. Ed. 45 (2006) 4473–4475.
[20] B. Rungtaweevoranit, A. Butsuri, K. Wongma, K. Sadorn, K. Neranon, C. Nerungsi, T. Thongpanchang, Tetrahedron Lett. 53 (2012) 1816–1818.
[21] C.B. Nielsen, J.M. Fraser, B.C. Schroeder, J. Du, A.J.P. White, W. Zhang, I. McCulloch, Org. Lett. 13 (2011) 2414–2417.
[22] R. Rieger, D. Beckmann, A. Mavrinskiy, M. Kastler, K. Müllen, Chem. Mater. 22 (2010) 5314–5318.
[23] N. Cheng, Y. Ma, Y. Liu, C. Zhang, C. Liu, Spectrochim. Acta, Part A 159 (2016) 262–268.
[24] (a) S. Wang, M. Kivala, I. Lieberwirth, K. Kirchhoff, X. Feng, W. Pisula, K. Müllen, Chem. Phys. Chem. 12 (2011) 1648–1657;
(b) B.C. Schroeder, C.B. Nielsen, Y.J. Kim, J. Smith, Z. Huang, J. Durrant, S.E. Watkins, K. Song, T.D. Anthopoulos, I. McCulloch, Chem. Mater. 23 (2011) 4025–4031.
[25] (a) F. Chérioux, L. Guyard, P. Audebert, Chem. Commun. (1998) 2225–2226;
(b) S. Kotha, K. Chakraborty, E. Brahmachary, Synlett 10 (1999) 1621–1623;
(c) J. Bras, S. Guillerez, B. Pépin-Donat, Chem. Mater. 12 (2000) 2372–2384;
(d) F. Chérioux, L. Guyard, Adv. Funct. Mater. 11 (2001) 05–309;
(e) Y. Geng, A. Fechtenkűtter, K. Müllen, J. Mater. Chem. 11 (2001) 1634–1641;
(f) T.M. Pappenfus, K.R. Mann, Org. Lett. 4 (2002) 3043–3046;
(g) S.A. Ponomarenko, S. Kirchmeyer, A. Elschner, B.-H. Huisman, A. Karbach, D. Drechsler, Adv. Funct. Mater. 3 (2003) 591–596;
(h) S. Inoue, S. Nischiguchi, S. Murakami, Y. Aso, T. Otsubo, V. Vill, A. Mori, S.J. Ujiie, Chem. Synop Res. (1999) 596–597.
[26] (a) F. van Bolhuis, H. Wynberg, E.E. Havinga, E.W. Meijer, E.G.J. Staring, Synth. Met. 30 (1989) 381–389;
(b) P.A. Chaloner, S.R. Gunatunga, P.B. Hitchcock, Acta Crystallogr., Sect. C 50 (1994) 1941–1942;
(c) M. Pelletier, F. Brisse, Acta Crystallogr., Sect. C 50 (1994) 1942–1943.
[27] Y. Jiang, D. Yu, L. Lu, C. Zhan, D. Wu, W. You, Z. Xie, S. Xiao, J. Mater. Chem. A 1 (2013) 8270–8279.
[28] (a) B. Wang, W. Liu, H. Li, J. Mai, S. Liu, X. Lu, H. Li, M. Shi, C.-Z. Li, H.J. Chen, Mater. Chem. A 5 (2017) 9396–9401;
(b) H. Liu, Z. Zhang, M. Huang, B. Zhao, J. Zhang, S. Tan, Synt. Met. 227 (2017) 122–130.
[29] A. Riaño, I. Arrechea-Marcos, M. Mancheño, A.J. Burrezo, P.M. de la Peña, A. Loser, S. Timalsina, A. Facchetti, A. Marks, T.J. Casado, J. Navarrete, J.T.L. Ortiz, R.o.P. Segura, Chem. Eur. J. 22 (2016) 6374–6381.
[30] Y. Chen, G.-Q. Liu, Y.-Y. Wang, P. Yu, Z. Liu, Q. Fang, Synth. Met. 162 (2012) 291–295.
[31] A. Molina-Ontoria, I. Zimmermann, I. Garcia-Benito, P. Gratia, C. Roldán-Carmona, S. Aghazada, M. Graetzel, M.K. Nazeeruddin, N. Martín, Angew. Chem., Int. Ed. 55 (2016) 6270–6274.
[32] X. Wu, Z. Zhang, H. Hang, Y. Chen, Y. Xu, H. Tong, L. Wang, Macromol. Rapid Commun. 38 (2017) 1700001.
[33] H.H. Bildirir, V.G. Gregoriou, A. Avgeropoulos, U. Scherf, C.L. Chochos, Mater. Horiz 4 (2017) 546–556.
[34] J. Zhang, S. Xie, X. Zhang, Z. Lu, H. Xiao, C. Li, G. Li, X. Xu, X. Chen, Z. Bo, Chem. Commun. 53 (2017) 537–540.
[35] H. Bildirir, D. Di Carlo Rasi, M.M. Wienk, R.A.J. Janssen, A. Avgeropoulos, V.G. Gregoriou, S. Allard, U. Scherf, L. Chochos, Macromol. Rapid Commun. 39 (2018) 1700629.
[36] Y. Wang, W. Xu, J. Yi, C. Zuo, Y. Gong, Y. Liu, W.-Y. Lai, W.J. Huang, Mater. Chem. A 6 (2018) 15977–15984.
[37] (a) W. Domagala, B. Pilawa, M. Lapkowski, Elecrochim. Acta 53 (2008) 4580–4590;
(b) J.L. Brédas, G.B. Street, Acc. Chem. Res. 18 (1985) 309–315.
[38] A. Ringk, A. Lignie, Y. Hou, H.N. Alshareef, P.M. Beaujuge, ACS Appl. Mater. Interfaces 8 (2016) 12091–12100.
[39] H. Wei, J. Ning, X. Cao, X. Li, L. Hao, J. Am. Chem. Soc. 140 (2018) 11618–11622.
[40] (a) A.N. Cammidge, R.J. Bushby, Handbook of Liquid Crystals, Wiley-VCH: Weinheim, 1998, pp. 693–784;
(b) S. Chandrasekhar, Handbook of Liquid Crystals, Wiley-VCH: Weinheim, 1998, pp. 749–780;
(c) N. Boden, B. Movaghar, Handbook of Liquid Crystals, Wiley-VCH: Weinheim, 1998, pp. 781–798;
(d) J. Wu, W. Pisula, K. Müllen, Chem. Rev. 107 (2007) 718–747;
(e) T. Kato, T. Yasuda, Y. Kamikawa, M. Yoshio, Chem. Commun. (2009) 729–739;
(f) S. Kumar, Liq. Cryst. 31 (2004) 1037–1059.
[41] (a) S. Laschat, A. Baro, N. Steinke, F. Giesselmann, C. Hagele, G. Scalia, R. Judele, E. Kapatsina, S. Sauer, A. Schreivogel, M. Tosoni, Angew. Chem., Int. Ed. 46 (2007) 4832–4887;
(b) S. Sergeyev, W. Pisula, Y.H. Geerts, Chem. Soc. Rev. 36 (2007) 1902–1929.
[42] R.J. Bushby, O.R. Lozman, Curr. Opin. Solid State Mater. Sci. 6 (2002) 569–578.
[43] (a) J. Cornil, V. Lemaur, J.P. Calbert, J.L. Bredas, Adv. Mater. 14 (2002) 726–729;
(b) V. Lemaur, D.A. Da Silva Filho, V. Coropceanu, M. Lehmann, Y. Geerts, J. Piris, M.G. Debije, A.M. Van de Craats, K. Senthilkumar, L.D.A. Siebbeles, J.M. Warman, J.L. Bredas, J. Cornil, J. Am. Chem. Soc. 126 (2004) 3271–3279;
(c) F. Xinliang, V. Marcon, W. Pisula, M.R. Hansen, J. Kirkpatrick, F. Grozema, D. Andrienko, K. Kremer, K. Müllen, Nat. Mater. 8 (2009) 421–426;
(d) J. Kirkpatrick, V. Marcon, K. Kremer, J. Nelson, D. Andrienko, J. Chem. Phys. 129 (2008) 094506.
[44] A.A. Demenev, S.H. Eichhorn, T. Taerum, D. Perepichka, S. Patwardhan, F.C. Grozema, L.D.A. Siebbeles, Chem. Mater. 22 (2010) 1420–1428.
[45] C.B. Nielsen, B.C. Schroeder, A. Hadipour, B.P. Rand, S.E. Watkinsc, I. McCulloch, J. Mater. Chem. 21 (2011) 17642–17645.
[46] (a) S. Loser, C.J. Bruns, H. Miyauchi, R.P. Ortiz, A. Facchetti, S.I. Stupp, T.J. Marks, J. Am. Chem. Soc. 133 (2011) 8142–8145;
(b) Y. Li, Q. Guo, Z. Li, J. Pei, W. Tian, Energy Environ. Sci. 3 (2010) 1427–1436.
[47] (a) Y.J. Cheng, S.H. Yang, C.S. Hsu, Chem. Rev. 109 (2009) 5868–5923;
(b) X. Zhao, X. Zhan, Chem. Soc. Rev. 40 (2011) 3728–3743.
[48] C.B. Nielsen, R.S. Ashraf, B.C. Schroeder, P. D'Angelo, Scott E. Watkins, K. Song, T.D. Anthopoulos, J. McCulloch, Chem. Commun. 48 (2012) 5832–5834.
[49] X. Zhao, D. Yang, H. Lv, L. Yin, X. Yang, Polym. Chem. 4 (2013) 57–60.
[50] C.B. Nielsen, R.S. Ashraf, M.D. Treat, B.C. Schroeder, J.E. Donaghey, A.J.P. White, N. Stingelin, I. McCulloch, Adv. Mater. 27 (2015) 948–953.
[51] M.L. Keshtov, A.R. Khokhlov, S.A. Kuklin, F.-C. Chen, E.N. Koukaras, G.D. Sharma, ACS Appl. Mater. Interfaces 8 (2016) 32998–33009.
[52] C.B. Nielsen, E.-H. Sohn, D.J. Cho, B.C. Schroeder, J. Smith, M. Lee, T.D. Anthopoulos, K. Song, I. McCulloch, ACS Appl. Mater. Interfaces 5 (2013) 1806–1810.
[53] B.C. Schroeder, S. Rossbauer, R.J. Kline, L. Biniek, S.E. Watkins, T.D. Anthopoulos, I. McCulloch, C.B. Nielsen, Macromolecules 47 (2014) 2883–2890.
[54] X. Guo, S.R. Puniredd, M. Baumgarten, W. Pisula, K. Müllen, J. Am. Chem. Soc. 134 (2012) 8404–8407.
[55] (a) H.J. Chen, Y.L. Guo, G. Yu, Y. Zhao, J. Zhang, D. Gao, H.T. Liu, Y.Q. Liu, Adv. Mater. 24 (2012) 4618–4622;
(b) I. Kang, T.K. An, J.-A. Hong, H.-J. Yun, R. Kim, D.S. Chung, C.E. Park, Y.-H. Kim, S.-K. Kwon, Adv. Mater. 25 (2013) 524–528;
(c) L.T. Dou, J. Gao, E. Richard, J.B. You, C.C. Chen, K.C. Cha, Y.J. He, G. Li, Y. Yang, J. Am. Chem. Soc. 134 (2012) 10071–10078;
(d) C. Kanimozhi, N. Yaacobi-Gross, K.W. Chou, A. Amassian, T.D. Anthopoulos, S. Patil, J. Am. Chem. Soc. 134 (2012) 16532–116325;
(e) J. Lee, A.-R. Han, J. Kim, Y. Kim, J.H. Oh, C. Yang, J. Am. Chem. Soc. 134 (2012) 20713–20721.
[56] A. Kojima, K. Teshima, Y. Shirai, T. Miyasaka, J. Am. Chem. Soc. 131 (2009) 6050–6051.
[57] Best Research-Cell Efficiencies (NREL, accessed 18 July 2019); https://www.nrel.gov/pv/assets/pdfs/best-research-cell-efficiencies.20190703.pdf.
[58] L. Meng, J. You, Y. Yang, Nature Commun. 9 (2018) 5265.
[59] G. Grancini, C.C. Roldán-Carmona, I. Zimmermann, E. Mosconi, X. Lee, D. Martineau, S. Narbey, F. Oswald, F. De Angelis, M. Graetzel, M.K. Nazeeruddin, Nature Commun. 8 (2017) 15684.
[60] (a) N. Arora, M.I. Dar, A. Hinderhofer, N. Pellet, F. Schreiber, S.M. Zakeeruddin, M. Grätzel, Science 358 (2017) 768–777;
(b) Y. Hou, X.Y. Du, S. Scheiner, D.P. McMeekin, Z.P. Wang, N. Li, M.S. Killian, H. W. Chen, M. Richter, I. Levchuk, N. Schrenker, E. Spiecker, T. Stubhan, N.A. Luechinger, A. Hirsch, P. Schmuki, H.P. Steinruck, R.H. Fink, M. Halik, H.J. Snaith, C.J. Brabec, Science 358 (2017) 1192–1197.
[61] (a) S.D. Stranks, P.K. Nayak, W. Zhang, T. Stergiopoulos, H.J. Snaith, Angew. Chem. Int. Ed. 54 (2015) 3240–3248;
(b) H.S. Jung, N.G. Park, Small 11 (2015) 10–25;
(c) M.M. Lee, J. Teuscher, Miyasaka T. Murakami, T.N. Snaith, H. J, Science 338 (2012) 643–647;
(d) J. Burschka, N. Pellet, S.J. Moon, R. Humphry-Baker, P. Gao, M.K. Nazeeruddin, M. Graetzel, Nature 499 (2013) 316–319;
(e) M. Liu, M.B. Johnston, H.J. Snaith, Nature 501 (2013) 395–398.
[62] J. Calbo, R. Viruela, J. Aragó, E. Ortí, Theor. Chem. Acc. 136 (2017) 73.
[63] I. García-Benito, I. Zimmermann, J. Urieta-Mora, J. Aragó, A. Molina-Ontoria, E. Ortí, N. Martín, M.K.J. Nazeeruddin, Mater. Chem. A 5 (2017) 8317–8324.
[64] R. Sanjaykumar, S.R. Suranagia, R. Singha, M. Kim, Dyes Pigments 163 (2019) 525–532.